JOURNAL OF GEOPHYSICAL RESEARCH, VOL. 115, C06020, doi:10.1029/2009JC005285, 2010

Nonlinear terms in storm surge predictions: Effect of tide and shelf geometry with case study from Hurricane Rita

João L. Rego[1,2] and Chunyan Li[1,3]

Received 14 January 2009; revised 29 January 2010; accepted 4 February 2010; published 24 June 2010.

[1] This study applied the finite volume coastal ocean model (FVCOM) to the storm surge induced by Hurricane Rita along the Louisiana-Texas coast. The model was calibrated for tides and validated with observed water levels. Peak water levels were shown to be lower than expected for a landfall at high tide. For low- and high-tide landfalls, nonlinear effects due to tide-surge coupling were constructive and destructive to total storm tide, respectively, and their magnitude reached up to 70% of the tidal amplitude in the Rita application. Tide-surge interaction was further examined using a standard hurricane under idealized scenarios to evaluate the effects of various shelf geometries, tides, and landfall timings (relative to tide). Nonlinearity was important between landfall position and locations within 2.5 × radius of maximum winds. On an idealized wide continental shelf, nonlinear effects reached up to 80% of the tidal amplitude with an S2 tide and up to 47% with a K1 tide. Increasing average depths by 4 m reduced nonlinear effects to 41% of the tidal amplitude; increasing the slope by a factor of 3 produced nonlinearities of just 26% of tide (both with a K1 tide). The nonlinear effect was greatest for landfalls at low tide, followed by landfalls at high tide and then by landfalls at midebb or midflood.

Citation: Rego, J. L., and C. Li (2010), Nonlinear terms in storm surge predictions: Effect of tide and shelf geometry with case study from Hurricane Rita, *J. Geophys. Res.*, *115*, C06020, doi:10.1029/2009JC005285.

1. Introduction

[2] A storm surge is an abnormal rise of sea surface height caused by atmospheric forcing, including the wind stress and atmospheric pressure at sea surface associated with extratropical cyclones and hurricanes or typhoons. "Storm tide" refers to the total water level including the effects of astronomical tide and surge. Storm surges have potentially devastating effects. In Bangladesh, hurricane-induced surges killed 250,000 people in November 1970 [*Flather*, 2001]. Hurricane Katrina's storm surge of August 2005 exceeded 9 m in several locations along the Mississippi coastline and became the costliest hurricane to ever strike the United States. It resulted in the death of over 1000 people in Louisiana and 200 in Mississippi [*Blake et al.*, 2006].

[3] We applied the finite volume coastal ocean model (FVCOM [*Chen et al.*, 2003]) to Hurricane Rita's storm tide of September 2005 and determined the flooding along the Louisiana-Texas coast in the northern Gulf of Mexico (GoM). The model was calibrated for tides and validated using water level data from USGS and NOAA. We sought to explain why peak surges were lower than linear superposition by examining the nonlinear terms in the governing equations. In addition, we conducted numerical experiments with a standard hurricane over idealized shelf geometries, by implementing simple tides and by varying the time of landfall in a set of simulations. Although there have been many storm surge studies in the literature, most of them did not consider the effect of tide on storm surge. These studies tend to fall into one of these categories: (1) disregarding tide altogether and resolving storm surge only [e.g., *Peng et al.*, 2004; *Weisberg and Zheng*, 2006a], (2) linearly superimposing storm surge and astronomical tide [e.g., *Graber et al.*, 2006], (3) either category 1 or 2 while acknowledging that the nonlinearity of surge and tide might be significant [e.g., *Bobanović et al.*, 2006; *URS Group*, 2006], and (4) running tide and surge simultaneously [e.g., *Peng et al.*, 2006b]. The studies in the last category, however, were often done without considering the details of nonlinear tide-surge interaction, a subject that we address in this study. Our results also provide new insight into how tidal speed and timing of landfall affect tropical storm surges for different shelf geometries.

[1]Coastal Studies Institute, Department of Oceanography and Coastal Sciences, School of the Coast and Environment, Louisiana State University, Baton Rouge, Louisiana, USA.

[2]Now at Division of Marine and Coastal Systems, Deltares, Delft, Netherlands.

[3]College of Marine Sciences, Shanghai Ocean University, Shanghai, China.

0148-0227/10/2009JC005285

2. Background Information

2.1. Importance of Wind and Shelf Geometry

[4] Wind stress is the dominant factor that generates the hurricane-induced storm surge in coastal seas [*Jelesnianski*, 1966; *Kohno et al.*, 2007]. Many numerical studies on storm

surges neglect the atmospheric pressure term [e.g., *Johns et al.*, 1985; *Jones and Davies*, 2007]. Since in the governing equations the wind stress term is divided by the total depth whereas the pressure gradient force is not, it follows that wind forcing is more important in shallower water [*Flather*, 2001].

[5] Under ideal and steady state conditions in deep water, the net transport of water by the wind occurs at a 90° angle to the right of the wind vector (northern hemisphere), and the alongshore component of wind stress causes a storm surge if the coast is to the right of the wind: the "bathystrophic storm tides" [*Gill*, 1982] or "Ekman setup" [*Shen and Gong*, 2009]. The across-shore component of wind stress becomes more important as water depth decreases, since the bottom stress diminishes the Coriolis tendency for transport to be to the right of the wind [*Weisberg and Zheng*, 2006b].

[6] In addition to the effect of wind stress, shelf geometry also has a significant impact on storm surge formation. Peak surges created by a given hurricane over wide continental shelves can be up to three times greater than those created over narrow shelves [*Jelesnianski*, 1972]. The importance of shelf bathymetry to coastal surges can be illustrated with a simple linear, steady state expression for the sea surface slope in equilibrium with a constant wind field [*Pugh*, 1987]: $\eta \propto LCW^2/H$, where η is the surge height at the coast, L is the shelf width, H is the average depth, W is the wind speed and C combines gravity, density and drag. Wind fields are rarely constant and such equilibrium is unlikely to be accurate, but this expression can be used to demonstrate that wind is more effective in raising the sea surface in shallow waters [e.g., *Resio and Westerink*, 2008].

2.2. Tide-Surge Interaction

[7] The effect of tide-surge interaction on extratropical surges affecting Europe due to nonlinear processes in shallow water regions has been known for some time (see reviews by *Heaps* [1983] and *Wolf* [2009]). Recently, *Jones and Davies* [2007, 2008] showed that tide-surge interaction significantly modified water elevations and currents at the time of the surge in the shallow regions of the Irish Sea.

[8] A tendency for extratropical storm surge maxima in the River Thames to occur most frequently on the rising tide was recognized, and theoretical solutions for the propagation of an externally forced tide and surge into an estuary of uniform section were developed by *Proudman* [1955, 1957]. However, the results did not agree with observations except in the immediate vicinity of the open boundary. *Rossiter* [1961] suggested that a key mechanism of interaction between tide and surge is mutual phase alteration: a negative surge would retard tidal propagation whereas a positive surge would increase the speed of tidal propagation and thus advance the high water.

[9] *Wolf* [1978] considered an analytical solution of two progressive waves along a semi-infinite channel. She showed that the interaction caused by quadratic friction was the largest, followed by the shallow water terms and advection terms. Interaction contributed by bottom friction increased with decreasing water depth and was proportional to the product of surge and tide. She concluded that surge height increased at rising tide and decreased at high tide due to this interaction. *Wolf* [1981] used a 1-D analytical model to show that the shallow water effect became dominant over quadratic friction for tidal amplitudes in excess of 3 m and in depths of 10 m or less. *Wolf* [2009] demonstrated that in the southern North Sea the surge peak tended to modify the predicted high tide due to the change of propagation speed when the surge modified the total depth.

[10] In a study of storm surges on the east coast of Great Britain, *Horsburgh and Wilson* [2007] suggested that surge peak always avoided high water (and low water). Their analysis of large, long-duration surge events confirmed that the surge generation was reduced at high water, and that increasing the tidal range reduced the chance of surge peaks to be near high water. But surges are not freely propagating Kelvin waves, and they respond very strongly to the change of meteorological conditions. Relaxing the meteorological forcing demonstrated that decay scales were of the order of 3 h or 100 km. These scales appeared to be highly dependent on location [*Horsburgh and Wilson*, 2007]. This study contradicted *Pugh and Vassie* [1980], who stated that there was little tide-surge interaction outside of estuaries.

[11] These results provided useful insight into the processes with tide and surge propagating together. The studies however did have some limitations such as the 1-D approximation and the exclusion of the advection terms. The North Sea studies did not include the effect of traveling weather systems, a factor absent in problems with free wave propagation [e.g., *Morey et al.*, 2006]. Thus, investigations of tide-surge interaction during tropical storms are necessary.

[12] *Johns et al.* [1985] studied tide-surge interaction for two cyclone surge events in the Bay of Bengal. Their numerical results showed larger nonlinear interaction in shallow water. The maximum elevation was 0.45 m below the expected linear superposition value. *Zhang et al.* [1993] showed that the greatest wind setup occurred during low and flood tides, when the nonlinear interaction strengthened the shoreward component of the current. Comparisons with observations showed that a simple linear superposition of astronomical tide with a separately computed surge might lead to errors of 1–2 m in surge prediction. *Qin et al.* [1994] concluded that including nonlinear tide-surge interactions in simulations considerably improved predictions of the total water level for Shanghai, especially in the vicinity of the highest total water level. Average Root Mean Square Errors for the highest storm tides were about 70% of those estimated using linear superposition.

[13] *Tang et al.* [1996] investigated the origin of nonlinear interaction along the Queensland coast of Australia by simulating surge and tide without advection in the momentum equations and replacing D (total depth) by H (undisturbed depth) in the pressure gradient and quadratic bottom friction terms. Having obtained surge residuals very similar to those using the complete equations, they concluded that the surge-tide interaction was mainly due to the nonlinear bottom friction. The effect of this nonlinear interaction was to always reduce the sea level below that obtained linearly (which was not consistent with *Wolf* [1981] or *Johns et al.* [1985]).

[14] *Kim et al.* [2008] showed that during Typhoon Ewiniar both surge and wave setup decreased while wave

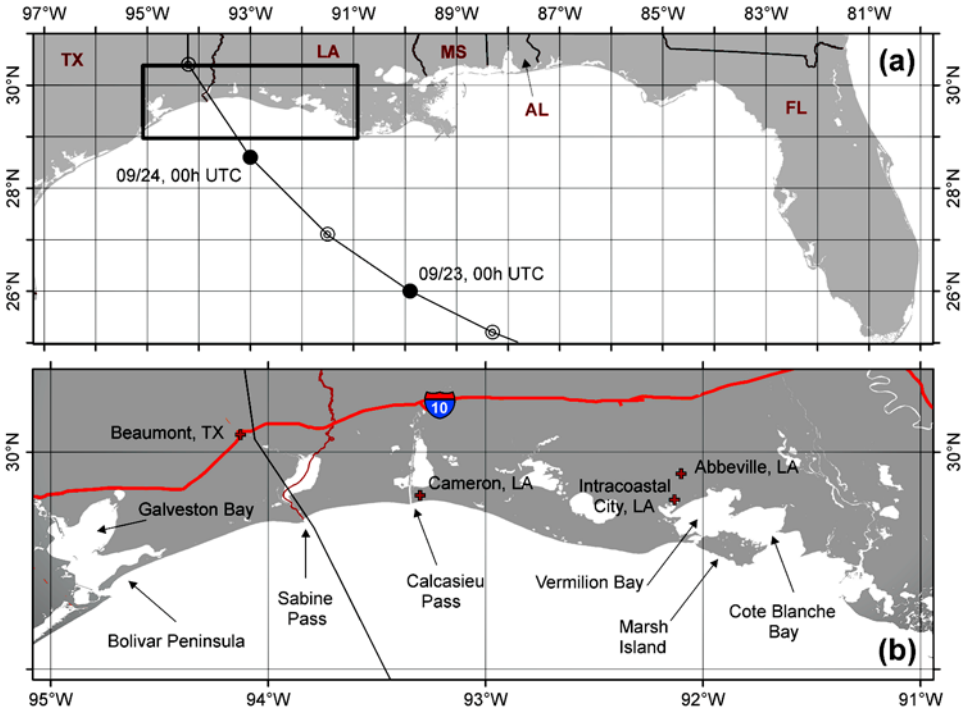

Figure 1. (a) Map of the northern Gulf of Mexico, including Hurricane Rita's track. The box indicates the zoom shown in Figure 1b. (b) Map of the Louisiana-Texas region most affected by Hurricane Rita, showing names of coastal features mentioned in the text.

heights increased at high tide (and vice versa at low water). This tendency increased with increasing tidal range.

[15] Surge-tide interactions in the Gulf of Mexico may be more complex than those in North Sea. One-dimensional considerations may be appropriate when the storm is large compared to the size of the shallow sea, but for smaller storms 2-D features become more important [*Welander*, 1961]. The surge in a 2-D situation may be generally smaller than that from a 1-D approximation, due to horizontal adjustments. Hurricanes are generally smaller and travel faster than extratropical storms, and 2- or even 3-D effects become more important. This is reflected in very different surge-to-tide period ratios: $(T_S/T_T)_{NorthSea} = 4$ and $(T_S/T_T)_{GoM} \sim 0.5$ (*Wolf* [1978] and *Rego* [2009], respectively). The present study provides a quantification of magnitude of nonlinear effects in time and space under hurricane conditions, and the determination of the effect of tide in the northern GoM.

2.3. Hurricane Rita

[16] The 2005 Atlantic Hurricane Season was exceptionally intense and Hurricane Rita made landfall near the Louisiana-Texas state border only three weeks after Hurricane Katrina had devastated the southeast Louisiana and Mississippi coastal regions. Rita intensified quickly upon entering the GoM, and attained Category 5 status and a peak sustained wind of 280 km/h within only 24 h. The recorded barometric pressure reached 897 mbar, the third lowest ever recorded for a tropical system in the Atlantic Basin at that time [*Knabb et al.*, 2006]. Hurricane Rita weakened as it approached the north-central coast of the GoM on 23 September, and became a Category 3 hurricane approaching landfall. It veered northward and moved ashore between Sabine Pass and Johnson's Bayou, Louisiana (Figure 1) at about 0800 UTC, 24 September with sustained winds of 195 km/h. Rita generated a substantial storm surge east of its landfall that reached 5–6 m, then weakened rapidly as it continued northward through east Texas [*Guidroz et al.*, 2006]. Hurricane Rita's landfall placed the western and central Louisiana coast within the right front quadrant of the storm, where maximum winds occurred. The highest high water marks (HWMs) measured by the Federal Emergency Management Agency (FEMA), ranging from 3.9 to 5.4 m, were along State Highway 82 in the area between Cameron and Grand Chenier [*URS Group*, 2006]. Storm surge in the open water was measured above 3 m along a distance of about 160 km from Johnson's Bayou to Marsh Island [*URS Group*, 2006]. Due east to Vermillion Bay, storm surges remained high and HWMs of up to 3.7 m were measured [*Guidroz et al.*, 2006].

3. Methods

3.1. Numerical Model: FVCOM

[17] We used the time-dependent, finite volume coastal ocean model (FVCOM, by *Chen et al.* [2003]) to simulate storm surge. FVCOM uses a "terrain following" sigma coordinate transformation in the vertical to accommodate irregular bathymetry, and a nonoverlapping unstructured triangular grid in the horizontal to resolve dynamics in regions with complex shorelines. After the Boussinesq and hydrostatic approximations the primitive equations for

momentum and mass conservation used in FVCOM are [*Chen et al.*, 2007]:

$$\frac{\partial uD}{\partial t}+\frac{\partial u^2D}{\partial x}+\frac{\partial uvD}{\partial y}+\frac{\partial u\omega}{\partial \sigma}-fvD= \\ =-gD\frac{\partial(\eta-\eta_a)}{\partial x}-\frac{gD}{\rho_0}\left[\frac{\partial}{\partial x}\left(D\int_{\sigma}^{0}\rho' d\sigma'\right)+\sigma\rho'\frac{\partial D}{\partial x}\right] \\ +\frac{1}{D}\frac{\partial}{\partial \sigma}\left(K_m\frac{\partial u}{\partial \sigma}\right)+DF_u \quad (1)$$

$$\frac{\partial vD}{\partial t}+\frac{\partial uvD}{\partial x}+\frac{\partial v^2D}{\partial y}+\frac{\partial v\omega}{\partial \sigma}+fuD= \\ =-gD\frac{\partial(\eta-\eta_a)}{\partial y}-\frac{gD}{\rho_0}\left[\frac{\partial}{\partial y}\left(D\int_{\sigma}^{0}\rho' d\sigma'\right)+\sigma\rho'\frac{\partial D}{\partial y}\right] \\ +\frac{1}{D}\frac{\partial}{\partial \sigma}\left(K_m\frac{\partial v}{\partial \sigma}\right)+DF_v \quad (2)$$

$$\frac{\partial \eta}{\partial t}+\frac{\partial uD}{\partial x}+\frac{\partial vD}{\partial y}+\frac{\partial \omega}{\partial \sigma}=0 \quad (3)$$

where u, v and ω are the x, y and σ velocity components, respectively; f is the Coriolis parameter; $D = h + \eta$ is the total water depth, where η and h are the surface elevation and reference depth below mean sea level, respectively; η_a is the sea level displacement induced by the "inverse barometer effect"; g is the gravitational acceleration; ρ_0 and ρ' are the reference and perturbation water densities, respectively; K_m is the vertical eddy viscosity coefficient; F_u and F_v represent the horizontal momentum diffusion terms in the x and y directions, respectively.

[18] The 2nd term on the right-hand side of equations (1) and (2) represent baroclinicity which was ignored in our simulations. The surface and bottom boundary conditions for u, v and ω are specified as

$$\left(\frac{\partial u}{\partial \sigma},\frac{\partial v}{\partial \sigma}\right)=\frac{D}{\rho_0 K_m}\left(\tau_{sx},\tau_{sy}\right),\omega=0\,\text{at}\,\sigma=0 \quad (4)$$

$$\left(\frac{\partial u}{\partial \sigma},\frac{\partial v}{\partial \sigma}\right)=\frac{D}{\rho_0 K_m}\left(\tau_{bx},\tau_{by}\right),\omega=0\,\text{at}\,\sigma=-1 \quad (5)$$

where (τ_{sx}, τ_{sy}) and (τ_{bx}, τ_{by}) are the x and y components of surface wind and bottom roughness stresses, respectively.

[19] FVCOM uses the modified Mellor and Yamada "level 2.5" turbulent closure scheme for vertical mixing [*Mellor and Yamada*, 1982; *Galperin et al.*, 1988] and *Smagorinsky*'s [1963] eddy parameterization for horizontal diffusion. Tide is forced at the open boundary by either specifying tidal constituents or elevation time series. Following the convention, the bottom stress is computed using the quadratic law

$$\left(\tau_{bx},\tau_{by}\right)=C_{db}\rho_0\sqrt{u^2+v^2}(u,v) \quad (6)$$

where the bottom drag coefficient, C_{db}, is determined by matching a logarithmic bottom layer to the model at the height of the first σ level above the bottom, i.e.,

$$C_{db}=\max\left\{\frac{k^2}{\left[\ln(1+\sigma_{kb-1})D/z_0\right]^2},\,BFRIC\right\} \quad (7)$$

where k = 0.4 is the von Kármán constant, z_0 is the bottom roughness parameter, *BFRIC* (typically between 0.002 and 0.004) is the minimum value for C_{db}, and $\sigma_{\mathrm{kb-1}}$ is the vertical level next to the bottom [*Weisberg and Zheng*, 2008]. The surface wind stress is

$$\left(\tau_{sx},\tau_{sy}\right)=C_{ds}\rho_a\sqrt{w_x^2+w_y^2}\left(w_x,w_y\right) \quad (8)$$

where (w_x, w_y) are the x and y components of the wind speed, respectively, ρ_a is the air density and C_{ds} is a drag coefficient dependent on wind speed, assumed constant when $\vec{V}_W > 25$ m/s [*Large and Pond*, 1981].

[20] In FVCOM a viscous boundary layer ($D_{\min}$) is added into the model at the bottom, to avoid the occurrence of singularity when the local water depth approaches zero and wet/dry points are redefined using a sum of D (the total depth) and $D_{\min}$. The grid is treated as a wet point for $D > D_{\min}$, otherwise it is a dry point [*Chen et al.*, 2008]. FVCOM is widely used in coastal ocean circulation studies forced by buoyancy, tide, atmospheric pressure gradients and winds [e.g., *Chen et al.*, 2007; *Huang et al.*, 2008; *Li et al.*, 2008]. Using FVCOM with flooding and drying driven by prototypical hurricane winds is a method that has been used successfully in storm surge simulations for this and other hurricane prone regions [*Weisberg and Zheng*, 2006a, 2006b, 2008; *Aoki and Isobe*, 2007; *Rego and Li*, 2009a, 2009b].

3.2. Grid for Hurricane Rita Simulations

[21] Our model domain extends from the Mexico-U.S. border to Apalachicola Bay in Florida, with a 1300 km open boundary covering water depths of 1000–3000 m (Figure 2a). A total of 178675 triangular cells with 90099 nodes comprise the horizontal; 2 sigma layers comprise the vertical. The grid resolution increases from 9 km on the open boundary toward the region of Hurricane Rita's impact. Grid resolution on the upper continental shelf between Bolivar Peninsula, TX and Marsh Island, LA (Figure 1) is about 500 m. The finest resolution (200 m) was applied on Sabine and Calcasieu Passes. The model domain in west Louisiana extended from the coastline to the 6 m elevation contour. Consequently, although this grid captured the entire northwestern GoM (submarine) bathymetry, it only included the (subaerial) topography for the area near Hurricane Rita's landfall. This limited our grid to studies of Hurricane Rita. In our applications, land cells had a 500–2000 m resolution and the flooding threshold depth, $D_{\min}$, was set to 0.1 m.

[22] Bathymetry data was a combination of the NGDC's U.S. Coastal Relief Model, the ETOPO-2 Global Relief model and LIDAR Atlas from Louisiana State University (LSU). In hurricane simulations, time steps of 0.6 and 6 s were used for the external and internal modes, respectively, and the model was run on the cluster computer of the Shell

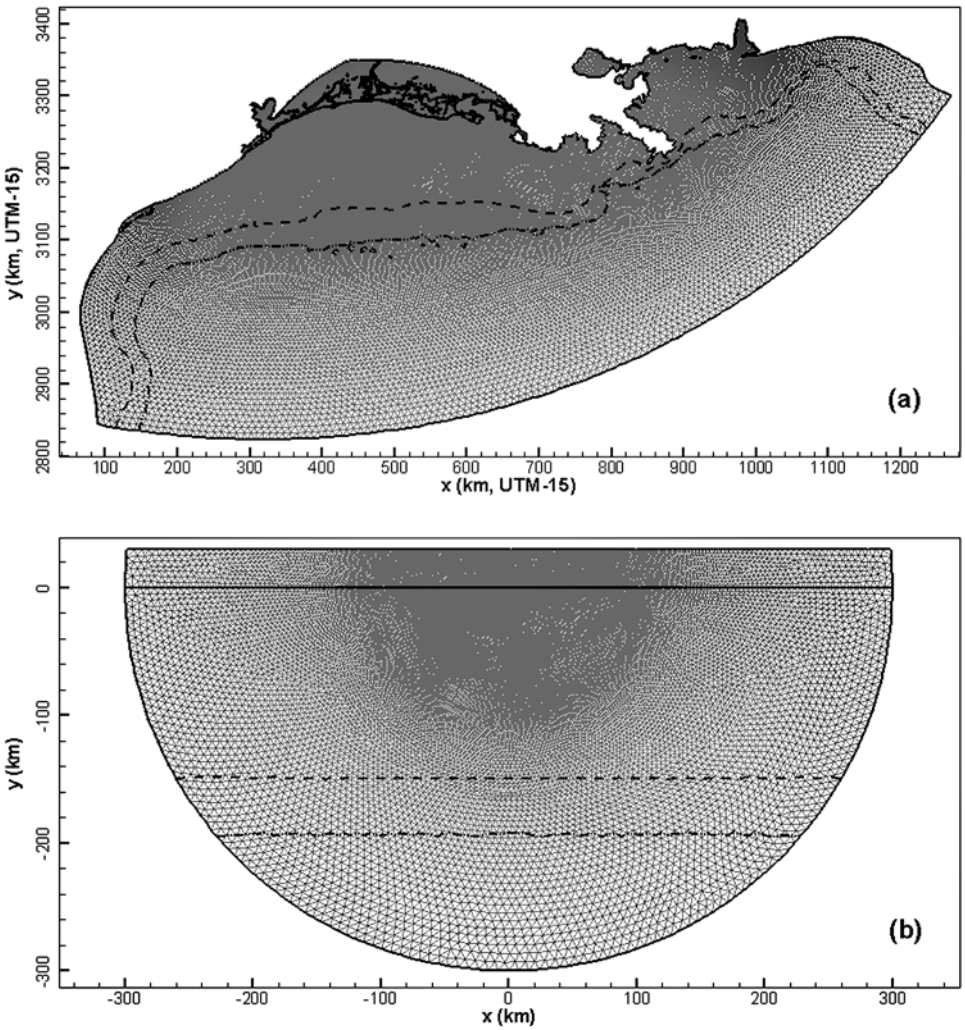

Figure 2. Grids used to simulate tide and storm surge: (a) Hurricane Rita simulations, with the Louisiana-Texas bathymetry. (b) Idealized simulations, with our representative Louisiana shelf geometry. The 0, 50, and 100 m depth contours are shown.

Coastal Environmental Modeling Laboratory of the School of the Coast and Environment at LSU. Forcing from the wind and tide is described in sections 3.3 and 3.4. The effects of air pressure, wave runup, and river discharge were not considered here.

3.3. Hurricane Wind Fields

[23] In a storm surge model, a common practice for creating hurricane wind fields [*Tang et al.*, 1996; *Peng et al.*, 2004, 2006a; *Weisberg and Zheng*, 2006a, 2006b] is to reconstruct the wind field by fitting the analytical cyclone model from *Holland* [1980]. The radial distribution of wind relative to the storm center and maximum wind speed are:

$$V_w = \sqrt{\frac{B(P_{amb} - MCP)}{\rho_a}\left(\frac{RMW}{r}\right)^B \exp\left(-\frac{RMW}{r}\right)^B} \quad (9)$$

$$V_{\max} = \sqrt{\frac{B(P_{amb} - MCP)}{\rho_a e}} \quad (10)$$

where r is the radial distance from the hurricane center; V_w is the wind speed as a function of r; ρ_a is the air density (= 1.15 kg/m^3); p_{amb} and MCP are the ambient and minimum central atmospheric pressures, respectively; e is the natural logarithm base (= 2.718…); RMW is the radius of maximum winds; $V_{\max}$ is the maximum sustained wind speed; and B is the "peakedness" storm scale parameter, $1.0 < B < 2.5$.

[24] In applying the *Holland* [1980] wind model, we used the gridded wind speed data from NOAA's Hurricane Research Division, the H*WIND data set [*Powell et al.*, 1996] to determine the (time-varying) parameters in equations (9) and (10). Many past studies only used a constant B without utilizing observed data [e.g., *Peng et al.*, 2006a; *Weisberg and Zheng*, 2006a]. Here we used a linear regression for B as a function of the RMW, based on the results from 4 major hurricanes making landfalls in the region and for which H*WIND data were available (Table 1). Terms (p_{amb} − MCP) and B were determined iteratively, using equations (9) and (10). We selected the combination of these terms that produced a wind profile with the smallest

Table 1. Hurricanes Used in Determining B = f(RMW)[a]

Hurricane	Year	Landfall	n
Lili	2002	Central Louisiana	10
Ivan	2004	Alabama	13
Katrina	2005	SE Louisiana, Mississippi	33
Rita	2005	Louisiana-Texas	30

[a]The number of H*WIND snapshots available is denoted as n.

Root Mean Square Error as compared to H*WIND's profile. Using 86 pairs of data, the resulting relation (R^2 of 72%) is $B = 0.0166RMW + 0.9735$, where B is dimensionless and RMW is given in km. To account for the forward motion of a tropical cyclone, representing the right-hand side (Northern Hemisphere) intensification of hurricane wind speeds, we used the method proposed by *Jelesnianski* [1966]. This correction ensured that the forward motion was realistically limited within the storm. This approach was also used in SLOSH for surge calculation [*Jelesnianski et al.*, 1992]. The forward motion velocity vector was computed every 3 h, from H*WIND's latitude and longitude information for Hurricane Rita. When gaps in H*WIND's data exceeded 3 h, we used the positions from UNISYS (2005 hurricane/tropical data for Atlantic, available at http://weather.unisys.com/hurricane/atlantic/2005H/index.html) to compute the forward velocities.

[25] The angle between the wind direction and the tangent to a circle concentric with the hurricane center due to friction (the "inflow angle") also contributed to the wind field asymmetry. Using constant values for the inflow angle, *Johns et al.* [1985] concluded that it had a negligible effect on coastal storm surge, whereas *Peng et al.* [2006b] concluded the opposite. Here, we set this angle to a constant 10° based on H*WIND data specific for Hurricane Rita.

[26] In summary, with a set of X, Y, RMW, V_{max}, and V_F for each H*WIND snapshot we assigned a wind vector for every cell in the model as a function of the distance to the hurricane center. Parametric wind fields were generated for the entire model domain using H*WIND data, and interpolated into 12 min intervals (the H*WIND observations were given at 3–9 h intervals). This method produced a better fit against observed winds while allowing for the simulation of idealized scenarios (sections 4.3–4.6). This approach is similar to the "spiderweb grid" method used in Delft3D-FLOW [*Deltares*, 2009].

3.4. Model Calibration for Tide

[27] To ensure that the model properly represented the characteristics of long-period wave propagation in our domain, a simulation of the tide was carried out with FVCOM. The model was run without surface wind forcing for 36 days, forced at its open boundary by 9 tidal constituents obtained from *Mukai et al.* [2002]. Hourly model outputs from the last 32 days were used for harmonic analysis of tidal constituents.

[28] Calibrating this application of FVCOM for tidal simulations consisted of varying the bottom friction coefficient, *BFRIC* (equation (7)), held constant throughout the entire domain. The bottom friction coefficient was varied between 0.0020 and 0.0050, and the best results were produced with *BFRIC* = 0.0040. Tidal constituent data (Table 2) were obtained from 14 long-term NOAA tidal stations, along with data from 3 WAVCIS stations (http://wavcis.csi.lsu.edu) located in areas impacted by Rita, covering east Texas to southeast Louisiana.

[29] The diurnal tide is dominant in the northern GoM, where major tidal constituents are O1, K1 (amplitudes of 0.12–0.17 m, with a minimum around southwest Louisiana) and M2 (0.03–0.15 m, with a maximum in southwest Louisiana). The largest errors occurred at Eagle Point, TX and Rainbow Bridge, TX, where FVCOM underrepresented the tide, and for Grand Isle, LA where it overestimated tidal amplitudes (Table 2). However, these stations were located either very far from the continental shelf, inside Galveston Bay and Sabine Lake, or very far from the landfall location of Rita. Semidiurnal amplitudes were smaller, and for M2 the stations with larger errors were Sabine Pass North, TX and Calcasieu Pass, LA, both located inside coastal passes

Table 2. Stations Used in Tidal Calibration[a]

	O1			K1			M2		
Station Name	Observed Amplitude	Amplitude	Phase	Observed Amplitude	Amplitude	Phase	Observed Amplitude	Amplitude	Phase
Corpus Christi, TX	0.162	+0.004	+0.62	0.160	+0.001	−0.15	0.083	−0.025	−0.08
Freeport, TX	0.147	+0.013	+0.64	0.152	+0.014	−0.11	0.096	−0.013	−0.17
Galveston Pleasure Pier, TX	0.161	+0.004	+0.70	0.171	+0.002	−0.03	0.139	−0.021	−0.16
Eagle Point, TX	0.114	−0.051	+1.41	0.117	−0.052	+0.65	0.034	−0.017	−0.25
Sabine Pass North, TX	0.123	−0.028	+0.19	0.132	−0.029	−0.42	0.123	−0.031	−0.26
Rainbow Bridge, TX	0.083	−0.054	+1.43	0.085	−0.054	+0.29	0.050	−0.033	−0.75
Calcasieu Pass, LA	0.136	+0.040	+0.24	0.144	+0.044	−0.50	0.146	+0.024	−0.16
CSI-03 (LSU)	0.154	+0.010	+0.94	0.169	+0.004	+0.25	0.126	−0.00	−0.10
Lawma, Amerada Pass, LA	0.121	+0.001	+1.10	0.126	+0.007	+0.26	0.084	−0.029	−0.41
CSI-05 (LSU)	0.143	+0.008	+0.83	0.149	+0.005	+0.21	0.027	+0.008	−0.47
CSI-06 (LSU)	0.142	+0.008	+0.87	0.149	+0.003	+0.21	0.024	+0.005	−0.53
Grand Isle, LA	0.114	+0.036	−0.63	0.114	+0.039	−1.25	0.013	+0.013	−1.00
Pilots Station East, SW Pass, LA	0.132	+0.014	+0.62	0.133	+0.015	−0.22	0.017	+0.005	−0.07
Gulfport Harbor, MS	0.157	+0.009	+0.75	0.172	+0.003	+0.03	0.035	+0.013	+0.29
Dock E, Port of Pascagoula, MS	0.149	+0.013	+0.03	0.170	−0.001	−0.61	0.027	+0.016	+0.32
Dauphin Island, AL	0.138	+0.002	−0.47	0.141	+0.002	−1.17	0.015	+0.013	+0.04
Panama City Beach, FL	0.141	+0.008	+0.88	0.145	+0.007	+0.03	0.034	−0.006	+0.59

[a]All stations are NOAA's except the three Coastal Studies Institute (LSU) stations indicated. Observed amplitude is shown in meters, then amplitude and phase differences (modeled – observed) between modeled and observed values, in meters and hours, respectively, for the three major tidal constituents.

Table 3. Stations Used in Hurricane Rita's Storm Surge Validation[a]

Station	Longitude, Latitude	Type	Maximum Observation Elevation (m)	Peak Error (m)	Peak Error (hours)
Galveston Pleasure Pier, TX	−94.788, 29.285	Offshore	0.94	−0.52	2.0
B15b (USGS)	−93.898, 29.765	Onshore	2.85	−0.19	−0.50
LC13 (USGS)	−93.753, 29.764	Onshore	3.24	0.15	−1.50
LC11 (USGS)	−93.583, 29.762	Onshore	4.54	0.20	−0.75
LC9 (USGS)	−93.471, 29.818	Onshore	4.21	−0.05	0.10
LC7 (USGS)	−93.403, 29.890	Onshore	3.40	0.20	−0.25
LC8a (USGS)	−93.329, 29.798	Onshore	4.07	0.65	−0.50
LC5 (USGS)	−93.228, 30.011	Inland	2.11	1.45	−8.50
LA12 (USGS)	−93.115, 29.786	Onshore	4.52	−0.01	0.50
LC8b (USGS)	−93.080, 29.871	Inland	2.25	1.00	−2.50
LA11 (USGS)	−93.015, 29.771	Onshore	4.47	−0.45	0.50
LA10 (USGS)	−92.676, 29.707	Inland	2.65	−0.16	0.20
LA9 (USGS)	−92.328, 29.745	Inland	2.02	0.54	−7.50
LA9b (USGS)	−92.193, 29.783	Onshore	3.27	−0.16	−3.75
LF5 (USGS)	−92.127, 29.886	Inland	3.07	0.30	−6.50
CSI-05 (LSU)	−90.533, 29.053	Offshore	1.18	−0.75	2.00
Grand Isle, LA	−89.957, 29.263	Offshore	1.11	−0.75	1.00
Pilots Station East, SW Pass, LA	−89.407, 28.932	Offshore	0.82	−0.30	1.50

[a]All stations are NOAA's except where indicated. Negative timing errors indicate modeled surge ahead of time. Positive peak errors indicate modeled value greater than observation.

where FVCOM underestimated and overestimated observed values, respectively, by about 15%. Other semidiurnal components were not fully captured in our application, but these were smaller amplitude constituents (S2 has 0.01–0.04 m amplitude on these stations; not shown). Typical amplitude prediction errors were about 0.01 m for the most important constituents. The errors for tidal phases rarely exceeded 1 h for all constituents at all stations. In a region dominated by diurnal tides, these errors were not significant.

3.5. Model Validation for Storm Surge

[30] Observations by *McGee et al.* [2006] provided data for Hurricane Rita's storm tide validation (Table 3). USGS deployed a total of 23 pressure sensors as Hurricane Rita approached, located along and near the coast ("onshore" in Table 3), from Sabine Pass, TX, to Abbeville, LA, covering locations about 100 m from the coast to about 45 km inland. Only 14 USGS stations were used here (Figure 3); the

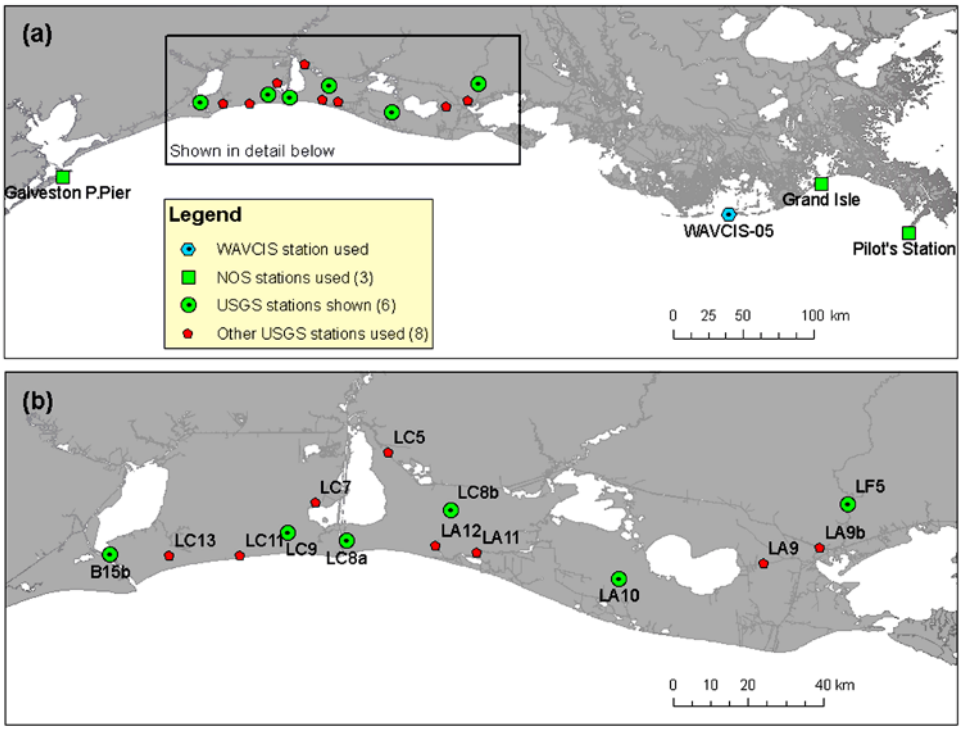

Figure 3. (a) Map of the region in the northern Gulf of Mexico most affected by Hurricane Rita, showing all stations used in surge validation. The box indicates the zoom shown in Figure 3b. (b) Detail of USGS stations used in surge validation.

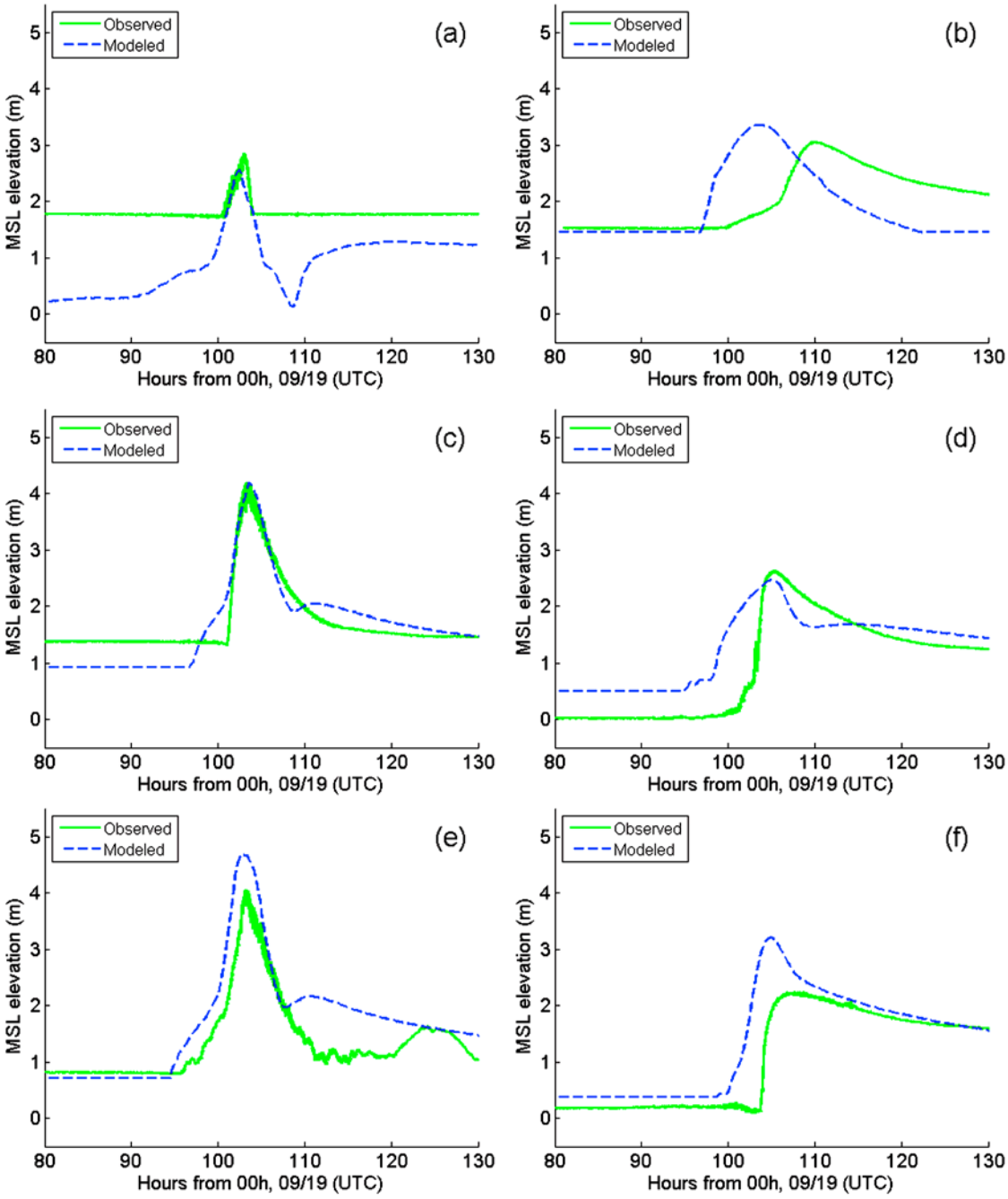

Figure 4. Modeled (FVCOM) versus observed (USGS) water levels for Hurricane Rita at stations (a) B15b, (b) LF5, (c) LC9, (d) LA10, (e) LC8a, and (f) LC8b. Model nodes were initially dry, except for the one in Sabine Pass (Figure 4a). Landfall for t = 104 h.

remainders were either too far north or located on small streams not resolved in the model.

[31] Data from three NOAA/NOS and one WAVCIS stations were also used for comparison with model results. The model skill seemed degraded at these offshore stations. Here, modeled peaks were smaller (by about 50%) than observations and about 1 h and 30 min late (Table 3). The three stations due east were far from the landfall location (350–500 km), while the station south of Galveston Bay, TX was in the left quadrant of the hurricane, where winds blowing from land were overestimated.

[32] Peak amplitude errors (model results versus USGS data) were typically ±0.2 m, where the storm tide was 3.5–4.5 m (e.g., Figure 4c), suggesting a 5% error. The exception was station LC8a (Figure 4e), where the model clearly overestimated the surge. This gave a 15% error. Station LC8a was located about 4 km inland from the GoM, on a "loop" of Calcasieu Pass.

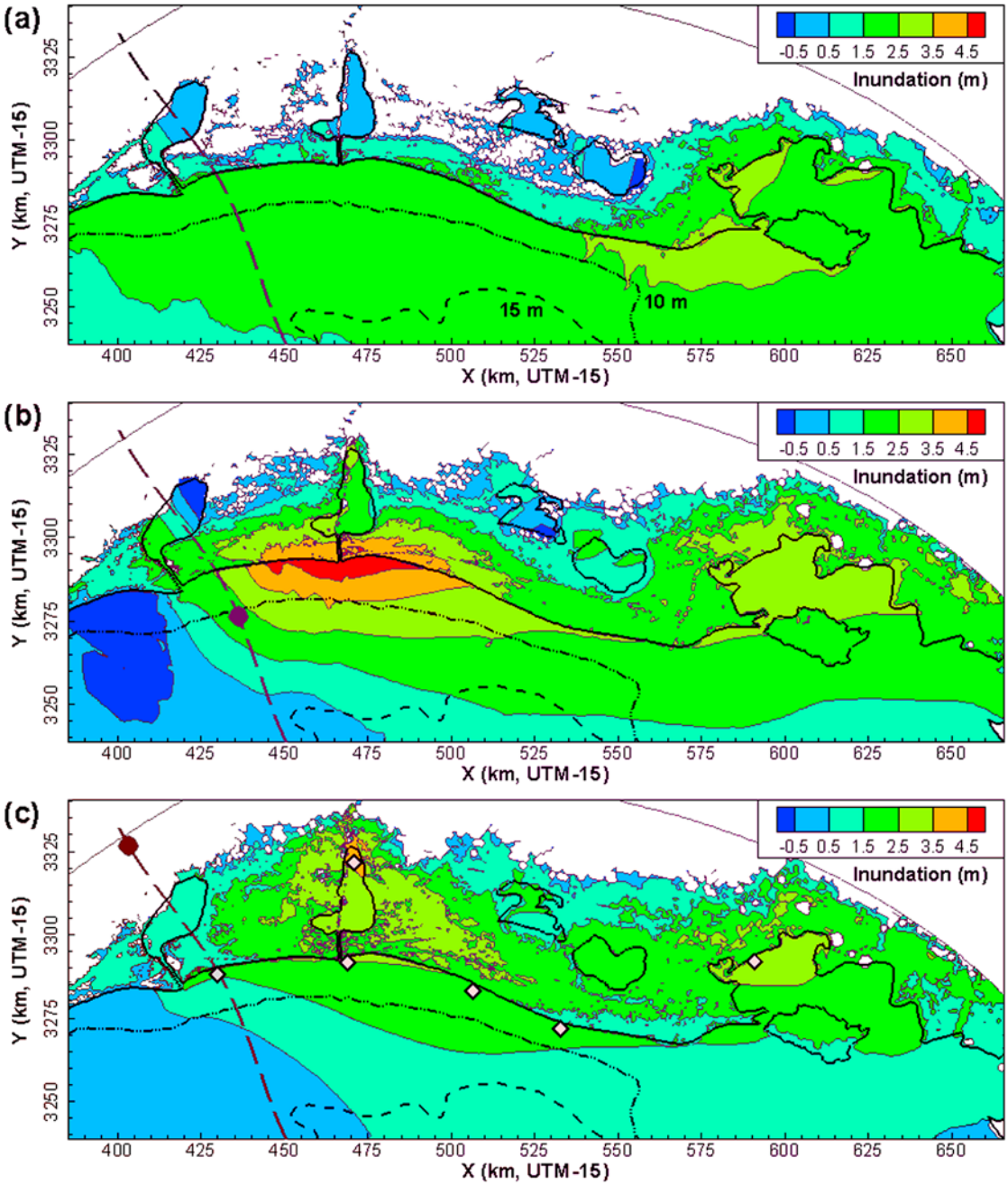

Figure 5. Inundation maps from model results: (a) 6 h before landfall, (b) 1 h before landfall, and (c) 2 h after landfall. Hurricane Rita made landfall at 0800 UTC, 24 September 2005. Hurricane track (long-dashed line) and position (dark gray circle) are shown. Figure 5c indicates six locations (gray diamonds) referred to in Figure 6.

[33] With respect to the timing of the storm tide, coastal results typically had a ± half hour shift (e.g., Figure 4a). Station LA9b yielded the worst comparison (not shown): the surge was estimated to arrive 3 h earlier than the data indicated (amplitude error was only 5%). This station was located near Intracoastal City, LA, about 3 km inland and near a network of channels not resolved in our grid. Inland stations did not do as well: either the peak elevations were overestimated (e.g., Figure 4f) or the peak arrived too early (e.g., Figure 4b), but in most stations only one of these issues was a problem. Station LA10 (Figure 4d) did not have these problems. Overall, the modeled surge curves were similar to observed curves and FVCOM reproduced the storm tide satisfactorily in the northern GoM.

4. Results and Discussion

4.1. Hurricane Rita's Storm Surge and Inland Flooding

[34] The model indicated that before landfall, at 0200 UTC, 24 September 2005, there was already significant coastal

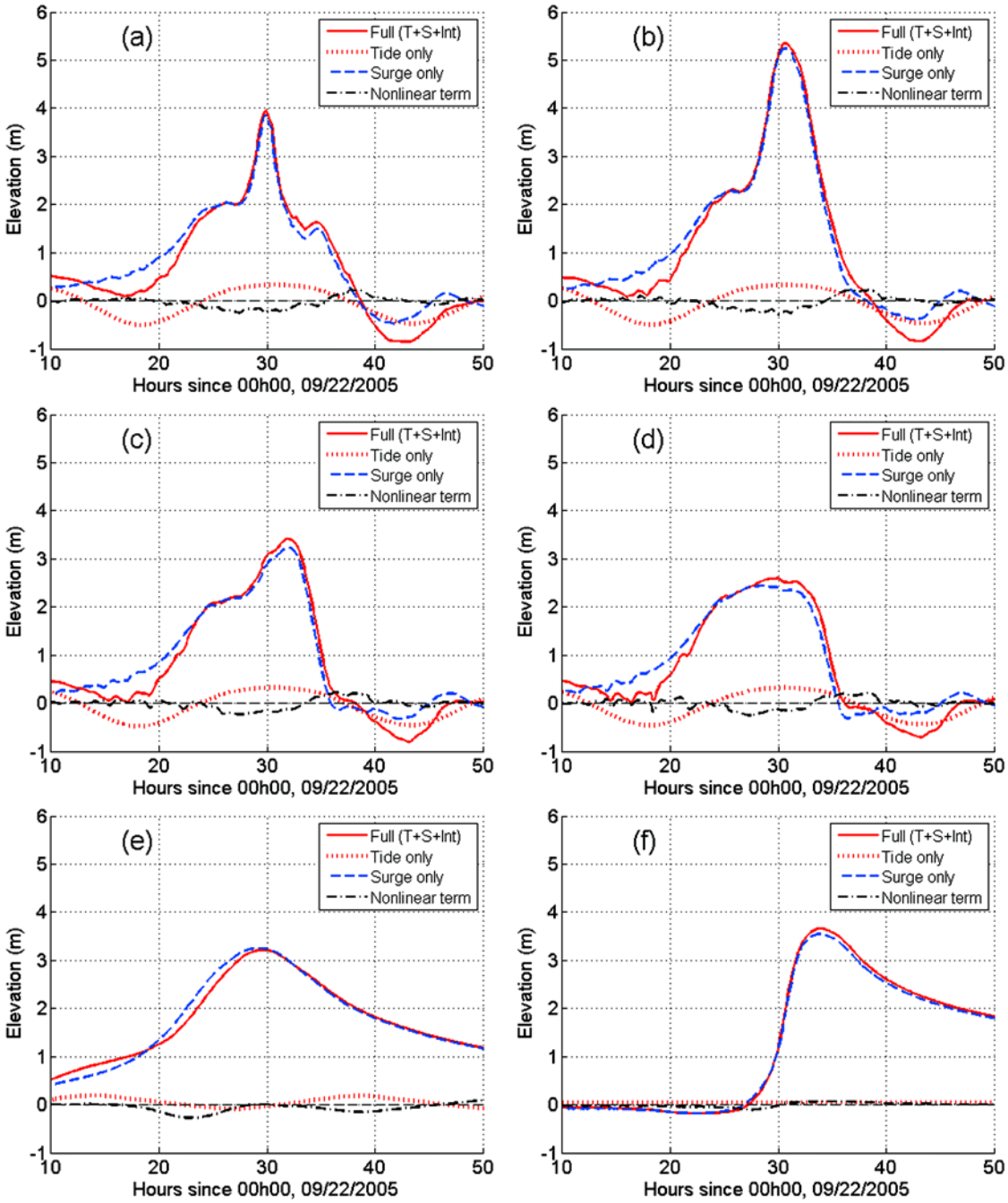

Figure 6. Water levels for locations indicated in Figure 5c: (a) near landfall, (b) 1 × RMW due east, (c) 2 × RMW due east, (d) 3 × RMW due east, (e) in Vermillion Bay, and (f) in Calcasieu Lake. Time shown as hours from 0000 UTC, 20 September 2005 (landfall at t = 32 h). Locations of Figures 6a–6d are at 4 m depth, and the other two are at 2.5 m depth. The four curves represent storm tide (solid line), pure tide (dotted line), surge only (dashed line), and the nonlinear interaction term (dot-dashed line). See Figure 5c for locations (gray diamonds).

inundation from Bolivar Peninsula, TX east to Cote Blanche Bay, LA. Inundation reached about 8–10 km inland eastward of Calcasieu Pass, where the storm tide was about 2 m (Figure 5a). At this early stage and given the hurricane's northwestward track, the cyclonic hurricane winds blew shoreward over Vermilion Bay and initial surges were highest in the shallow water around Marsh Island (Figure 5a). In Vermillion Bay the storm tide peaked almost 2.5 h before Hurricane Rita's landfall, and here the water levels had a relatively slow rise and fall (Figure 6e). The observed USGS water levels for stations LF5 (Figure 4b) and LA9 (not shown), however, suggested that the modeled inland flooding speed in this area was overestimated. This was attributed to the bottom coefficient not taking into account the effect of vegetation over wetland and flooded low-lying land (hindcast simulations of Hurricane Rita using SLOSH

Table 4. Gradients of the Typical Continental Shelf Tested

	Distances From Shore (km)
To 50 m isobath (upper shelf gradient = 0.333×10^{-3})	150
To 100 m isobath (midshelf gradient = 1.11×10^{-3})	195
To 1000 m isobath (continental slope gradient = 12.9×10^{-3})	265

and ADCIRC had similar inland issues [*URS Group*, 2006; *Guidroz et al.*, 2006]). At the point of impact the storm tide curve reached 4 m about 2 h before landfall (Figure 6a). In this location the local winds never really blew perpendicular to the shore; rather, they switched very quickly from easterly to westerly, causing the lower and briefer surge.

[35] The highest water levels (at about 5.35 m) did not occur where the point of maximum winds on the coastline (1 RMW due east), but rather at about 1.1 × RMW right of landfall (Figures 5b and 6b). This can be explained by the funneling effect caused by Calcasieu Pass. The storm surge curve here was broader and the "bulge" that dominated the rising water until about 6 h prior to landfall was also present. This represented the bathystrophic surge superseded by the oncoming cross-shore winds. At about 2 × RMW due east of landfall the surge curve was similar (Figure 6c): although the peak was considerably reduced, the bathystrophic surge peak of 2.2 m was almost the same as near the RMW. Farther east the surge peaks decreased even further (Figure 6d). Here the shore configuration relative to the hurricane track considerably decreased the onshore component of the wind, and surges peaked at only 2.6 m (Figure 6d).

[36] Two hours after landfall, flooding reached 30–50 km inland. At this time the highest water levels (at about 2.5 m) were still located near Calcasieu Pass, but surge spread east and west along the shore as well as over the land (Figure 6c). At the upstream part of Calcasieu Lake the storm tide peaked at 3.6 m, 2 h after landfall (Figure 6f). The water levels did not fall below 1.5 m for more than 30 h after landfall. The posthurricane receding stage lasted for several days. This is because (1) there was no wind reinforcement to push water back (gravity "spreading" became the restoring force) and (2) unlike the flooding stage when widespread coastal surges of above 2 m inundated everywhere over the land, receding waters only flowed through the existing narrow passes [*Rego and Li*, 2009b; *Li et al.*, 2009].

4.2. Effects on Nonlinear Tide-Surge Interaction

[37] Hurricane Rita made its landfall near high tide. To separate the storm tide into astronomical tide, surge residuals and the interaction component, simulations were run for tide-only and surge-only scenarios. As shown in Figure 6, in which the nonlinear interaction term was computed by $\eta_I = \eta_{T+S} - (\eta_T + \eta_S)$. The calculation showed a negative interaction term ($\eta_I < 0$) near the peak surge (Figures 6a–6d). Nonlinearity decreased the peak storm tide along the shoreline east of landfall, where the storm tide was highest (Figures 6a–6d).

[38] To test if this pattern held under a different tide, the same wind forcing was used with a landfall occurring at low tide, and with a doubled tidal amplitude. The same pattern occurred for the nonlinear effect: the nonlinear term opposed the tide by enhancing storm tide heights when the tide was near its minimum.

[39] Our results indicated that nonlinearity was significant, reaching up to 66%–75% of the tidal amplitude. Other authors previously reached similar conclusions qualitatively [*Zhang et al.*, 1993; *Horsburgh and Wilson*, 2007; *Wolf*, 2009]. Here we have provided more in-depth quantitative analysis, as described in sections 4.5 and 4.6.

4.3. Idealized Simulations

[40] To better understand the sensitivity of surge generation to local tide and continental shelf geometry, different scenarios were examined. A standard hurricane was defined, for use in all of the simulations. The only variable for the hurricane was the landfall timing relative to the tide. The RMW was set to 40 km, consistent with a Category 3 or 4 hurricane [*Hsu and Yan*, 1998]. Its maximum sustained wind speed was set to 40 m/s, representing a medium-strength hurricane [*Resio and Westerink*, 2008]. Hurricane moving speed was set to 5 m/s, the average from those in Table 1.

[41] A typical profile representing the continental shelf of central Louisiana was defined (Table 4). The distance from shore to the 50 m isobath was set to 150 km and the shelf break (as measured by the 100 m isobath) 45 km further offshore. The gradient for the continental slope, from the shelf break down to the 1000 m depth, was the same for all cases (Table 4).

[42] An idealized computational grid was developed for these profiles (Figure 2b). The model domain formed a semicircle centered at the point of landfall ($x = 0$, $y = 0$), with the open boundary located 300 km away from the center. Depth was 0.0 m along the $y = 0$ line and decreased linearly to $z = -10$ m northward to the $y = 30$ km line. Positive depths, representing "wet" nodes, were increased by 1.0 m, to reduce wetting and drying during tidal runs. There were a total of 50234 triangular cells with 25317 nodes in the horizontal and 2 sigma layers in the vertical. Grid resolution was 500–2000 m in most cells (8 km at the open boundary).

[43] The synthetic tides had an amplitude of 0.50 m, slightly larger than the observed tide on the Louisiana-Texas shelf. The synthetic tide in the idealized experiments was diurnal, except for scenario C which had a semidiurnal tide. Scenario B had a minimum depth of 5.0 m, allowing an evaluation of the effect of deeper water over the shelf (Table 5). For each simulation the standard hurricane was forced to make landfall at significant tidal phases: high tide, ebb, low tide, and flood (where ebb and flood were defined based on water levels rather than currents). This set of

Table 5. Four Storm Tide Scenarios Tested With Standard Hurricane[a]

Scenario	Depth Added	Tidal Period
A	1 m	K1 (23.94 h)
B	5 m	K1 (23.94 h)
C	1 m	S2 (12.00 h)

[a]Shelf geometry is summarized in Table 4 (representative of Louisiana's west continental shelf). The depth added immediately seaward of the shoreline (to the entire shelf, thereby maintaining the desired slopes) is also shown. Tidal amplitude was 0.5 m in all cases.

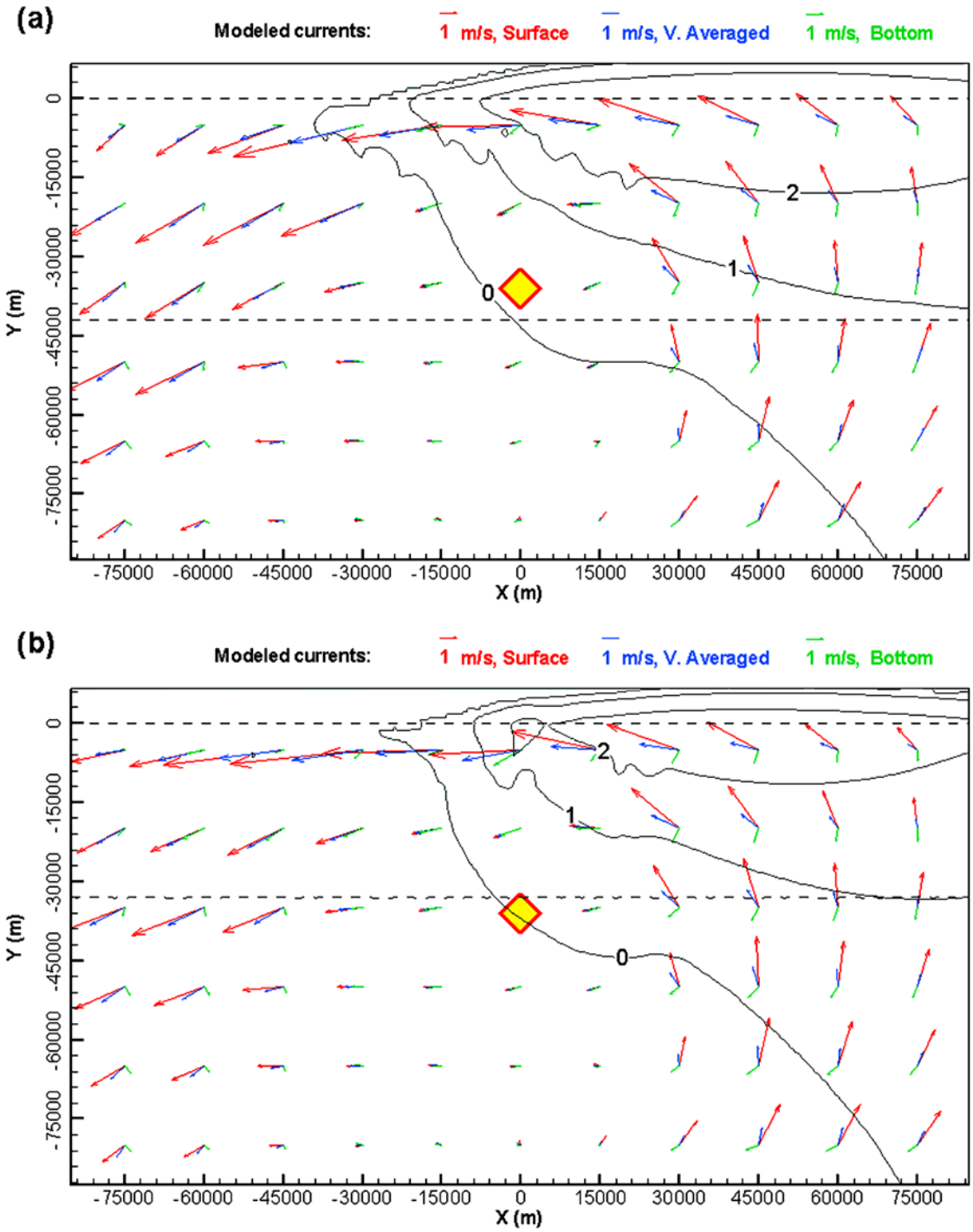

Figure 7. Surge-only currents in idealized simulations for (a) scenario A (K1 tide, wide shelf) and (b) scenario B (the same only 4 m deeper). Red, blue, and green vectors represent surface, depth-integrated, and bottom currents, respectively. Coastal currents are shown 2 h before landfall, for the standard hurricane of RMW = 40 km. The yellow diamond indicates the center of the hurricane. Currents were resampled into regularly spaced 15 km vectors for clarity (grid resolution was 500–2000 m). Dashed lines are the 0 and 15 m isobaths. Solid lines represent inundation heights, in meters.

$3 \times 4 = 12$ simulations on a simplified coast with simple tides provided insight into how shelf depth as well as tidal timing and tidal period affect hurricane-induced storm tides.

4.4. Vertical Structure of the Flow

[44] A storm surge represents a balance of vertically integrated pressure gradient force (the surface slope) with the difference of the surface and bottom stresses. The

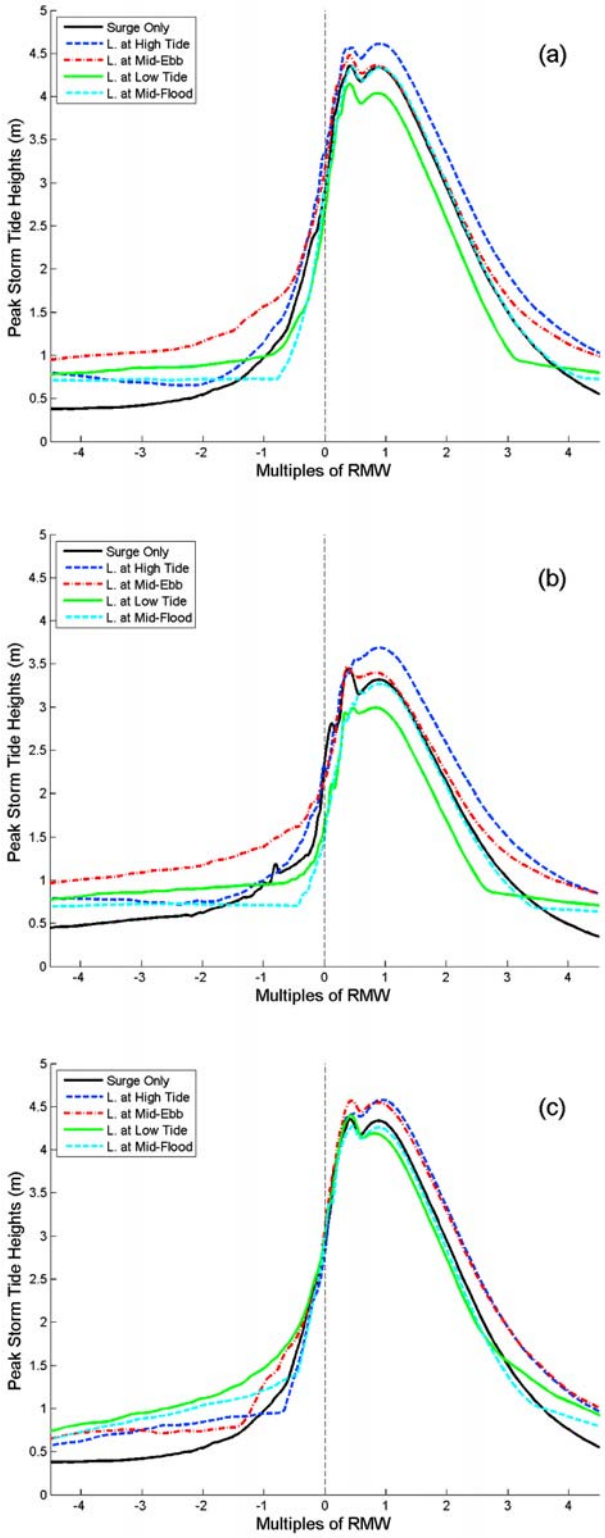

Figure 8. Peak storm tide elevations along $y = 0$: (a) scenario A, (b) scenario B, and (c) scenario C (Table 5). Different locations have peaks at different times. Surge only is shown as a dark solid line; other lines represent simulations including tides, for which hurricane made landfalls at different times. Abscissa is distance right (positive) and left (negative) of landfall, in multiples of RMW (= 40 km).

surface stress is from the wind; the bottom stress is where 2-D and 3-D models differ: in the 2-D case this is based on the depth-averaged velocity whereas in the 3-D case it is based on the near-bottom velocity. Hence, a 2-D model tends to overestimate bottom stress and underestimate surge height. This may not be problematic in hindcast because the effective bottom drag coefficient can be calibrated. However, the different drag coefficients are not physically the same and important physics may not be resolved due to compensation of errors [*Weisberg and Zheng*, 2008]. Our model application accounted for this by using two equally spaced sigma layers in the vertical, whereas most storm surge applications in the literature were run in 2-D. In our application FVCOM included an integrated bottom layer (matching a logarithmic layer to the model at the height of the first σ level above the bottom) and the top layer was forced at the surface by wind stress.

[45] In the area of interest (Figure 7) each layer had 0.5–8 m thickness; that is, velocities represented estimates at 0.25–4 m above (or below) the seabed (or water surface). Comparing scenario A (Figure 7a) with scenario B (Figure 7b), surface currents in the former were stronger and had larger across-shore components. The shallower scenario A led to a stronger surge asymmetry, in that surge elevations were higher to the right of the hurricane and lower to its left, as compared to a scenario only 4 m deeper.

[46] Bottom currents on the right-hand side of the hurricane were directed to the left of the surface currents, from about 90 to 180°. Here the bottom current vectors were against the surface elevation gradient. This was the bottom return current described by *Welander* [1961] for the "quasi-steady surge with vertical circulation." Thus the bottom stress had a shoreward component, which contributed to increase the setup against shore. This 3-D effect appeared to be a counterintuitive, enhancing effect on coastal surge. This is another example that three-dimensional models are preferable over 2-D models for simulating storm surges [see also *Weisberg and Zheng*, 2008].

4.5. Effects of Nonlinear Tide-Surge Interaction: Idealized Storm Tides

[47] The peak height difference between low- and high-tide landfalls may serve as a first approximation for nonlinear effects: nonlinear effects were greatest for scenario C (0.38 m, Figure 8c), followed by scenario A (0.58 m, Figure 8a) and scenario B (0.70 m, Figure 8b). These differences should equal the tidal range (1 m in this case) without interaction.

[48] All surge and storm tide peak curves were greater to the right of the landfall point, as expected. For scenario A, surge-only peaks reached 4.35 m at $x = 0.45 \times$ RMW and $x = 0.9 \times$ RMW, and passed 2 m in $-0.3 \times \text{RMW} < x < +2.6 \times$ RMW (Figure 8a). Note that for $x < -1.5 \times$ RMW and $x > +3.8 \times$ RMW all of the peak storm tides were above the surge-only line. This is because these storm tide maxima refer to the local high tide, which did not exist in the pure surge simulation. Indeed, the timing of peak storm tide gradually deviated from the timing of peak pure surge, approaching the time of local high tide, far from $x = +$RMW. Given this increase in complexity, but mostly because nonlinearity greatly decreased away from the highest surges, we focused on the $-0.5 \times \text{RMW} < x < +2.5 \times$ RMW interval.

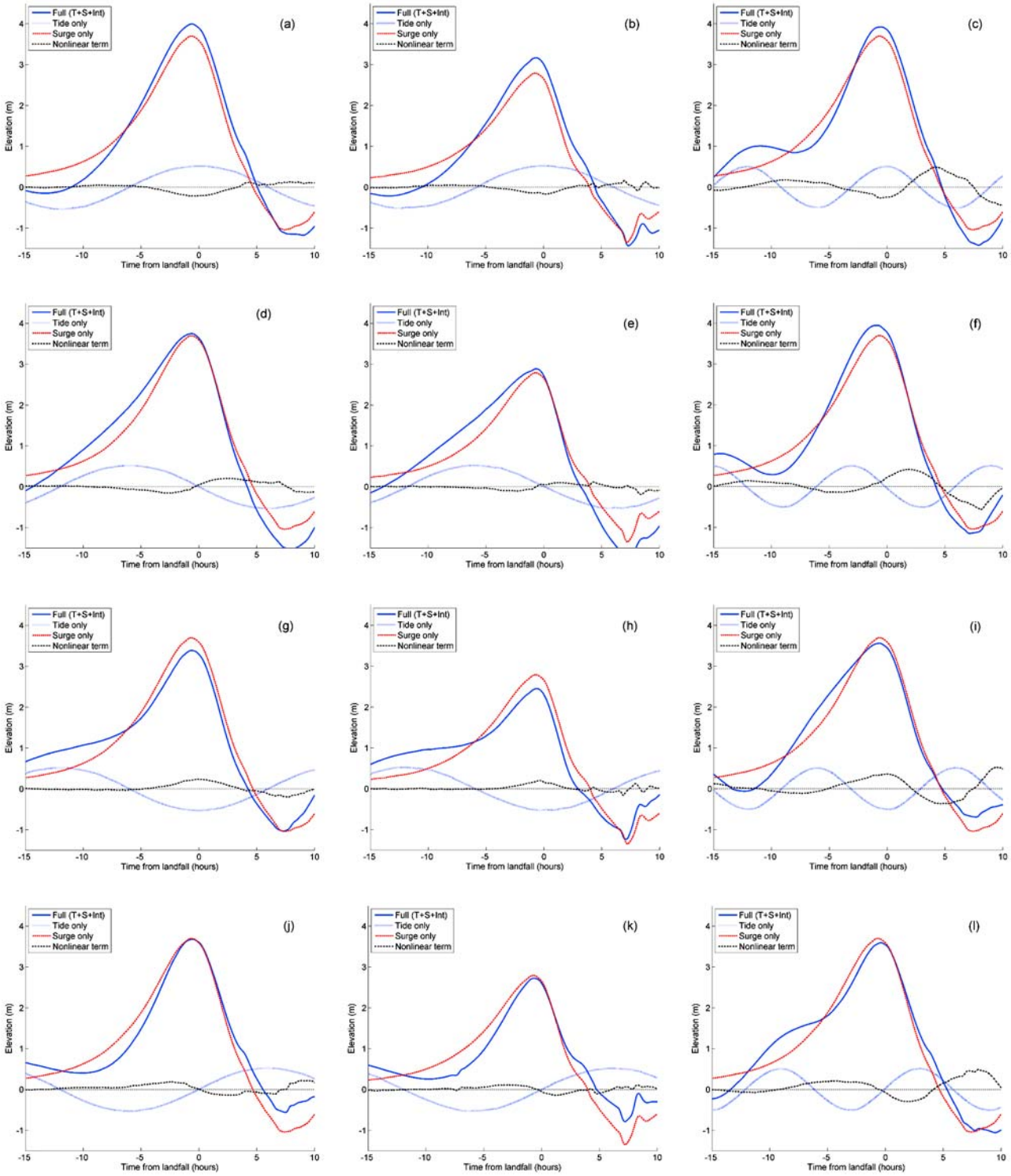

Figure 9. Water levels at x = +0.9 × RMW. Results for landfall at (a–c) high tide, (d–f) midebb, (g–i) low tide, and (j–l) midflood for scenario A (Figures 9a, 9d, 9g, and 9j), scenario B (Figures 9b, 9e, 9h, and 9k), and scenario C (Figures 9c, 9f, 9i, and 9l). The four curves have the same meanings as in Figure 6. All landfalls at t = 20 h. Nodes used to create Figure 9 (4 km offshore) are at different depths: 2.4 m for scenarios A and C and 6.4 m for scenario B.

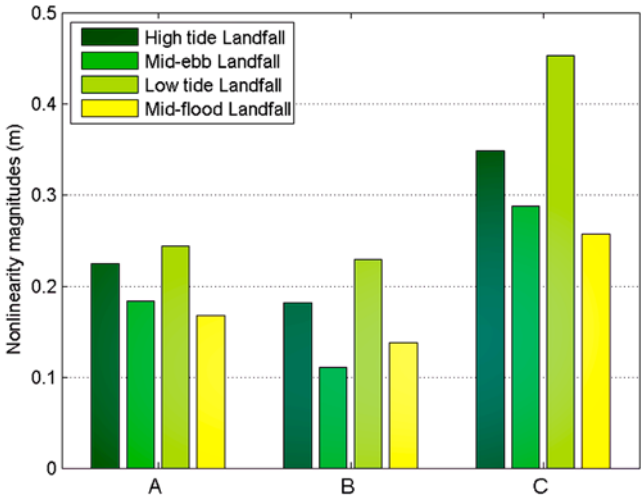

Figure 10. Magnitudes of nonlinear term maxima for idealized simulations, near x = +RMW for the four different landfall timings (four different color bars). Abscissa represent different scenarios (Table 5). For landfalls at low or high tide, only the nonlinear term during peak surge is shown. For landfalls at midebb or midflood the average magnitude of two peaks is shown.

This was consistent with *Li* [1988], whose approximate analytical solution with both astronomical tide and a forced meteorological surge gave a greater nonlinear effect in the center of the forced wave.

[49] Figure 9 summarizes the three scenarios, for each of the four types of landfall timings, at x = +0.9 × RMW. Peak pure surge was highest (3.67 m) at 0.9 × RMW to the right of landfall. This distance, shorter than RMW in a straight coastline, was due to the nonzero inflow angle used in the hurricane wind field (resulting in strongest winds hitting land slightly west of geometric RMW). For scenario A, the effect of nonlinearity for landfalls at high or low tide was to change peak storm tide heights to about 0.30 m lower and higher, respectively, than peak pure surge (Figures 9a and 9g). Nonlinearity reduced its maximum, between peak surge and highest/lowest tide (these are separated by about 30 min), thus the resulting storm tide curves were similar to the surge-only curves, for rising and falling stages. The second nonlinearity peak, at the time of lowest surge, created negative storm tides with the same elevation as the pure surge (opposing the tide).

[50] For landfalls at midebb or midflood, peak storm tide heights were the same as pure surge, suggesting negligible nonlinearity. However, a linear addition of surge and tide for a landfall at midflood (Figure 9j) produced a curve with a gentler slope before landfall and a steeper decline afterward, whereas for a landfall at midebb (Figure 9d) linearly adding tide and surge resulted in a curve with a steeper slope ahead of landfall and a gentler decline afterward. The nonlinear effect was relevant (opposing the tide) in the ±5 h around peak storm tide, and merely altered the "shape" of storm tide curves.

[51] At 2 × RMW right of landfall (not shown), storm surge was about 70% of peak surges. Here the effect of nonlinearity for high- or low-tide hurricane landfall was to produce peak storm tides about 0.4 m lower and higher, respectively, than peak pure surge, indicating a decrease of nonlinearity as local pure surges decreased. The effect of nonlinearity for all landfall timings tested was the same for scenarios B and A, albeit with a decreased magnitude: a change in shape for ebb or flood tide landfalls and a change in peak amplitude for high- or low-tide landfalls.

[52] Scenario C yielded the greatest nonlinearities. Although peak pure surges were the same as scenario A, peak nonlinear effects at these locations were about 50% greater in scenario C. Contrary to the diurnal tide scenarios, a landfall at midebb produced a peak storm tide higher than the pure surge (Figure 9f). For landfalls at low or midflood tides, the peak storm tides were comparable, both about 0.12 m lower than pure surge (Figures 9i and 9l).

[53] Figure 10 shows peak magnitudes of the nonlinear effect along $y = 0$, averaged along $0.75 \times \mathrm{RMW} < x < 1.25 \times \mathrm{RMW}$. Figure 10 presents a quick summary of nonlinear magnitudes, for the tested range of shelf average depths, tidal speed and timing of landfall. Nonlinear effects reached up to about 80% of the tidal amplitude for scenario C, about 47% for scenario A, and about 41% for scenario B (averaging high- and low-tide values). With the same broad and shallow shelf and the same peak storm surge value, 3.7 m, scenario A had a K1 tide and scenario C had an S2 tide. The latter produced much larger nonlinear effect. For all scenarios tested the nonlinear effect was greatest for landfalls at low tide, followed by landfalls at high tide (10%–30% smaller) and then by those cases with landfalls at midebb or midflood (further 30%–45% smaller).

4.6. Nonlinear Residuals in the Momentum Equations

[54] Variations in the nonlinear bottom friction terms, $C_d u\sqrt{u^2+v^2}/(h+\eta)$ and $C_d v\sqrt{u^2+v^2}/(h+\eta)$, and nonlinear momentum advection (terms 2–4 in equations (1) and (2)), generate tide-surge interaction in shallow water and influence the distribution of energy between tide and surge. The change in friction and advective terms, taken as the difference between tide with surge and tide only plus surge only, reveals the nonlinear residuals in the simulations. Our work was similar to that of *Tang et al.* [1996] in that we evaluated the importance of the quadratic bottom friction (equation (6)). *Jones and Davies* [2008] did a similar study on extratropical surges in the Irish Sea. Their model results indicated that these nonlinear residuals were significantly larger (by a factor of 100) in shallow waters as compared to deep waters (1.8 m and 45 m depths in their example). Over shallow waters, their bottom friction term peaked at about 5×10^{-4} m s^{-2}, while their advection term peaked at about 5×10^{-5} m s^{-2}.

[55] Here we examine in detail results at two locations, "point 1" and "point 2" (located 1 × RMW and 2 × RMW to the right of landfall, respectively) for both real and idealized geometries, and for low- and high-tide landfalls (Figure 11). Time series of the various terms in the y momentum equation (not shown) indicated that bottom friction and advective terms were the most significant to the right of landfall, together balancing the pressure gradient force. In the simulation for Hurricane Rita storm surge with the realistic Louisiana-Texas grid, the friction and advection terms had the same order of magnitude. In the idealized simulations, advection was about 5 times smaller than friction. This was expected. As indicated by *Li* [2006] and *Li et al.* [2008],

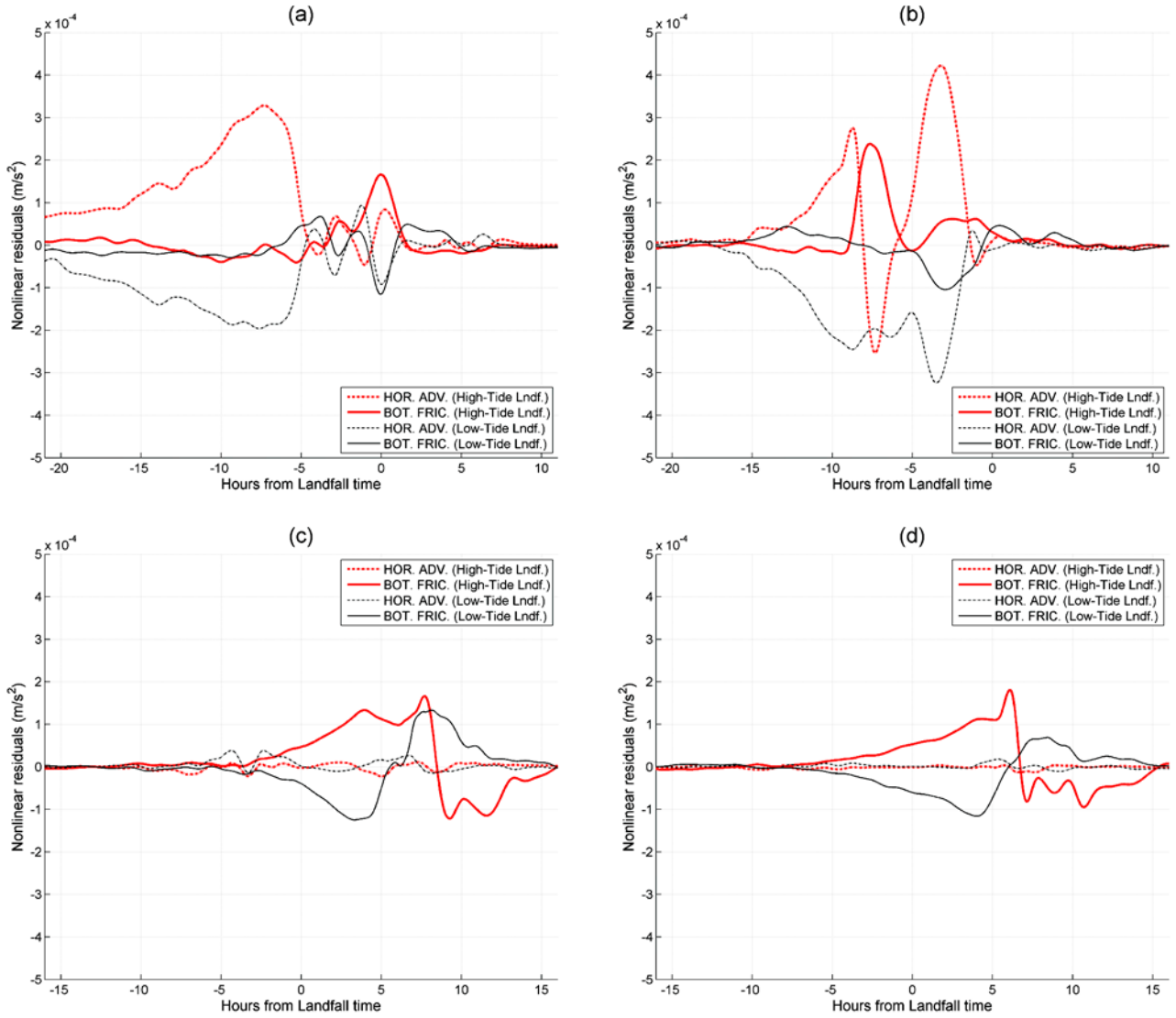

Figure 11. Changes in the y momentum of the two major nonlinear components: bottom friction ($C_d v\sqrt{u^2 + v^2}/(h + \eta)$, solid lines) and horizontal advection ($u\partial v/\partial x + v\partial v/\partial y$, dashed lines), both in m s^{-2}. Each plot shows nonlinear residuals for landfalls at low tide (fine, black lines) and high tide (thick, red lines): Hurricane Rita model results at points (a) 1 and (b) 2 and scenario A's results, also for points located (c) 1 × RMW and (d) 2 × RMW to the right of landfall. These are the same points used in Figures 6 and 9 (over depths of about 4 m in the LA-TX grid and 2.5 m in the idealized grid).

advection tends to be much larger when there is a complication of bathymetry and curvature of the coastlines. As much as 45%–70% of the nonlinearity can be from advection when such complication exists. In the along-shelf momentum balance, all terms were an order of magnitude smaller than that in the across-shelf direction.

[56] Figure 11 shows a time series of the difference in these terms for the realistic (Figures 11a and 11b) and idealized (Figures 11c and 11d) cases, with low- and high-tide landfalls. For the Louisiana-Texas simulations, changes in nonlinear terms show significant temporal and spatial variability. Much like in the work by *Jones and Davies* [2008], nonlinear residuals peaked at about 2–4 × 10^{-4} m s^{-2}, also with many fluctuations without a clear pattern. Because of the fast movement of the hurricane, the local wind-forced currents varied quickly, and the advective and frictional terms changed significantly in time and space. In our simulations the advection term clearly dominated over the bottom friction term, indicating a higher degree of complexity. Comparing the low- and high-tide landfall curves on each plot, they tended to "mirror" each other, but with considerable noise.

[57] Not surprisingly, time series of nonlinear residuals from the idealized cases (Figures 11c and 11d) show less variability. Bottom friction clearly dominated over advection, which was very small. Here the friction nonlinear residuals peaked at only about 2 × 10^{-4} m s^{-2}. The effect of nonlinearities on overall storm tides (sections 4.2 and 4.5) was not that different between idealized and realistic simulations. This is attributed to the less oscillating behavior of the bottom friction residuals for the idealized scenarios as compared to the advective residuals for the realistic simulations. The

reason for the tendency of low- and high-tide landfall curves to "mirror" each other is also clearer.

[58] The variability with landfall timing can be appreciated by considering the influence of changes in bottom stress produced by tide. Since the bottom stress ($C_d vU/D$) depends on current magnitude U and total water depth $D = h + \eta$, even if η and U were constant, the influence of the stress would vary significantly as h changes rapidly nearshore. For a high-tide landfall, η increases, and so for a constant U the bottom stress decreases. In a pure surge simulation this reduces C_d, leading to an increase in surge amplitude. However, in a combined tide and surge calculation, U depends on both the storm surge current and tidal current. Therefore any reduction in bottom stress due to an increase in η in a combined tide-surge simulation can be offset by an increase in U, with an associated increase in bottom stress and reduction in surge energy.

5. Summary

[59] An application of FVCOM to storm surge induced by Hurricane Rita in September 2005 was implemented and the resulting inland flooding along the Louisiana-Texas coast studied. The simulated storm surge was verified using the USGS measurements in coastal and inland locations. From point of landfall to approximately 3 × RMW due east, peak storm tide reached 5 m.

[60] This study showed that along the coast, the locations east of landfall would experience nonlinearities opposing the tide, reducing storm tide heights when the tide was at rising stages. These locations would experience nonlinearities enhancing the storm tide during ebbing or close to low tide. For low- or high-tide landfalls, nonlinearity effects were constructive and destructive to total storm tide, respectively. Nonlinearities were significant, reaching up to about 70% of the tidal amplitude in both cases.

[61] In the second part of this study a systematic approach was used, forcing a typical hurricane on different shelf geometries for different tides and tidal timings (relative to landfall). Compared to the case with a "standard" hurricane hitting a wide shelf with a 1 m minimum depth, increasing the minimum depth to 5 m decreased the peak pure storm surge to about 75%. The analysis of surface and bottom currents showed how the shallower scenario led to a stronger surge asymmetry (higher surge elevations to the right of the hurricane and lower to its left).

[62] When tides were included in the simulations, the nonlinear interaction was important in the region along the coastline $-0.5 \times \mathrm{RMW} < x < +2.5 \times \mathrm{RMW}$ (with landfall at $x = 0$). This is where surges were higher and local peak storm tides coincided with local peak pure surges. For landfalls at midebb or midflood the main nonlinear effect was to oppose the tide in the 5 h before and after peak storm tides, generating storm tide curves with moderately different shapes but having the same peak height (as a linear superposition of surge and tide). For landfalls at high or low tide the nonlinear effect opposed the tide; that is, peak storm tide heights were lower and higher, respectively, than a linear superposition.

[63] Nonlinear effects reached up to 80% of the tidal amplitude on a wide shelf under a semidiurnal tide. This demonstrated the effect of amplification of nonlinearity over a wide shelf: the semidiurnal tide had larger nonlinear effect compared to the diurnal tide because the former had a shorter wavelength and "sensed" the shelf as being wider when the same geometry was used. With diurnal tides, nonlinear effects reached up to 47% for a wide shelf and 41% for a shelf 4 m deeper. The nonlinear effect was the greatest for landfalls at low tide, followed by landfalls at high tide and then landfalls at mid-ebb or mid-flood. Not accounting for such tide-surge interaction may result in a significant underestimation for a landfall at low tide.

[64] The variation in storm tide was produced by nonlinear effects of bottom friction and momentum advection due to the presence of the tide. Our analysis showed that the nonlinear residuals of advection dominated in the realistic simulations, while the nonlinear residuals of the quadratic bottom friction dominated in the idealized simulations (consistent with the findings by *Li et al.* [2008]). Because bottom friction was the most important nonlinear term, a possible variation in bottom drag coefficient would most likely influence the result. It would be desirable to allow a spatially variable drag coefficient for similar simulations to examine the impact to the results. While there were applications in which lower values were used "offshore" and higher values for shallower waters [e.g., *Retana*, 2008], our study produced a good validation with an overall "high" drag value (like, e.g., *Jones and Davies* [2008]), probably because our focus was on nearshore areas.

[65] **Acknowledgments.** The first author was funded by the Portuguese "Fundação para a Ciência e Tecnologia" doctoral fellowship 28815/2006. Changsheng Chen (University of Massachusetts–Dartmouth) kindly shared the FVCOM code. We also thank Lianyuan Zheng (University of South Florida) for helpful discussions about the code. We also acknowledge the support of NSF (OCE-0554674), NOAA (NA06NPS4780197) for NGoMEX, and NOAA (NA06OAR4320264-06111039) to the Northern Gulf Institute. The contributions from two anonymous reviewers have greatly improved this manuscript.

References

Aoki, A., and A. Isobe (2007), Application of finite volume coastal ocean model to hindcasting the wind-induced sea-level variation in Fukuoka Bay, *J. Oceanogr.*, *63*(2), 333–339, doi:10.1007/s10872-007-0032-7.

Blake, E. S., E. N. Rappaport, J. D. Jarrell, and C. W. Landsea (2006), The deadliest, costliest, and most intense United States tropical cyclones from 1851 to 2005 (and other frequently requested hurricane facts), *NOAA Tech. Memo., NWS TPC-4*, 48 pp., Syst. Dev. Off., Natl. Weather Serv., Silver Spring, Md.

Bobanović, J., K. R. Thompson, S. Desjardins, and H. Ritchie (2006), Forecasting storm surges along the east coast of Canada and northeastern US: The storm of 21 January 2000, *Atmos. Ocean*, *44*(2), 151–161, doi:10.3137/ao.440203.

Chen, C., H. Liu, and R. C. Beardsley (2003), An unstructured grid, finite-volume, three-dimensional, primitive equation ocean model: Application to coastal ocean and estuaries, *J. Atmos. Oceanic Technol.*, *20*, 159–186, doi:10.1175/1520-0426(2003)020<0159:AUGFVT>2.0.CO;2.

Chen, C., H. Huang, R. C. Beardsley, H. Liu, Q. Xu, and G. Cowles (2007), A finite-volume numerical approach for coastal ocean circulation studies: Comparisons with finite difference models, *J. Geophys. Res.*, *112*, C03018, doi:10.1029/2006JC003485.

Chen, C., J. Qi, C. Li, R. C. Beardsley, H. Lin, R. Walker, and K. Gates (2008), Complexity of the flooding/drying process in an estuarine tidal-creek salt-marsh system: An application of FVCOM, *J. Geophys. Res.*, *113*, C07052, doi:10.1029/2007JC004328.

Deltares (2009), *User Manual: Delft3D-FLOW: Simulation of Multi-Dimensional Hydrodynamic and Transport Phenomena, Including Sediments*, 644 pp., Delft, Netherlands.

Flather, R. A. (2001), Storm surges, in *Encyclopedia of Ocean Sciences*, edited by Steele, J. H., S. A. Thorpe, and K. K. Turekian, pp. 2882–2892, Academic, San Diego, Calif.

Galperin, B., L. H. Kantha, S. Hassid, and A. Rosati (1988), A quasi-equilibrium turbulent energy model for geophysical flows, *J. Atmos. Sci.*, *45*, 55–62, doi:10.1175/1520-0469(1988)045<0055:AQETEM>2.0.CO;2.

Gill, A. E. (1982), *Atmosphere-Ocean Dynamics*, 661 pp., Academic, New York.

Graber, H. C., V. J. Cardone, R. E. Jensen, D. N. Slinn, S. C. Hagen, A. T. Cox, M. D. Powell, and C. Grassl (2006), Coastal forecasts and storm surge predictions for tropical cyclones: A timely partnership program, *Oceanography*, *19*(1), 130–141.

Guidroz, W. S., G. W. Stone, and D. Dartez (2006), Hurricane Rita, 2005: Assessment of a storm-induced geological event along the southwestern Louisiana coast and adjacent interior marsh, *Trans. Gulf Coast Assoc. Geol. Soc.*, *56*, 229–239.

Heaps, N. S. (1983), Storm surges, 1967–1982, *Geophys. J. R. Astron. Soc.*, *74*, 331–376.

Holland, G. J. (1980), An analytic model of the wind and pressure profiles in hurricanes, *Mon. Weather Rev.*, *108*, 1212–1218, doi:10.1175/1520-0493(1980)108<1212:AAMOTW>2.0.CO;2.

Horsburgh, K. J., and C. Wilson (2007), Tide-surge interaction and its role in the distribution of surge residuals in the North Sea, *J. Geophys. Res.*, *112*, C08003, doi:10.1029/2006JC004033.

Hsu, S. A., and Z. Yan (1998), A note on the radius of maximum wind for hurricanes, *J. Coastal Res.*, *14*(2), 667–668.

Huang, H., C. Chen, G. W. Cowles, C. D. Winant, R. C. Beardsley, K. S. Hedstrom, and D. B. Haidvogel (2008), FVCOM validation experiments: Comparisons with ROMS for three idealized barotropic test problems, *J. Geophys. Res.*, *113*, C07042, doi:10.1029/2007JC004557.

Jelesnianski, C. P. (1966), Numerical computations of storm surges without bottom stress, *Mon. Weather Rev.*, *94*(6), 379–394, doi:10.1175/1520-0493(1966)094<0379:NCOSSW>2.3.CO;2.

Jelesnianski, C. P. (1972), SPLASH (Special Program To List Amplitudes of Surges From Hurricanes): 1. Landfall storms, *NOAA Tech. Memo., NWS TDL-46*, 56 pp., Syst. Dev. Off., Natl. Weather Serv., Silver Spring, Md.

Jelesnianski, C. P., J. Chen, and W. A. Shaffer (1992), SLOSH: Sea, lake, and overland surges from hurricanes, 71 pp., Natl. Weather Serv., Silver Spring, Md.

Johns, B., A. Rao, S. Dube, and P. Sinha (1985), Numerical modelling of tide surge interaction in the Bay of Bengal, *Philos. Trans. R. Soc. London, Ser. A*, *313*, 507–535, doi:10.1098/rsta.1985.0002.

Jones, J. E., and A. M. Davies (2007), Influence of non-linear effects upon surge elevations along the west coast of Britain, *Ocean Dyn.*, *57*(4–5), 401–416, doi:10.1007/s10236-007-0119-0.

Jones, J. E., and A. M. Davies (2008), On the modification of tides in shallow water regions by wind effects, *J. Geophys. Res.*, *113*, C05014, doi:10.1029/2007JC004310.

Kim, S. Y., T. Yasuda, and H. Mase (2008), Numerical analysis of effects of tidal variations on storm surges and waves, *Appl. Ocean Res.*, *30*(4), 311–322, doi:10.1016/j.apor.2009.02.003.

Knabb, R. D., D. P. Brown, and J. R. Rhome (2006), Tropical cyclone report: Hurricane Rita, 18–26 September 2005, 33 pp., Natl. Hurricane Cent., Miami, Fla.

Kohno, N., K. Kamakura, H. Minematsu, Y. Yorioka, K. Hisashige, E. Shinizu, Y. Sato, A. Fukunaga, Y. Taniwaki, and S. Tanijo (2007), The mechanism of the storm surges in the Seto inland sea caused by Typhoon Chaba (0416), *Tech. Rev., 9*, Reg. Spec. Meteorol. Cent. Tokyo–Typhoon Cent., Tokyo.

Large, W., and S. Pond (1981), Open ocean momentum flux measurements in moderate to strong winds, *J. Phys. Oceanogr.*, *11*, 324–336, doi:10.1175/1520-0485(1981)011<0324:OOMFMI>2.0.CO;2.

Li, C. (1988), Theoretical research on nonlinear interaction of free tide wave and forced surge (in Chinese with English abstract), *Mar. Forecasts*, *5*(1), 1–5.

Li, C. (2006), Modeling of bathymetry locked residual eddies in well-mixed tidal channels with arbitrary depth variations, *J. Phys. Oceanogr.*, *36*, 1974–1993, doi:10.1175/JPO2955.1.

Li, C., C. Chen, G. Guadagnoli, and I. Y. Georgiou (2008), Geometry induced residual eddies in estuaries with curved channel-observations and modeling studies, *J. Geophys. Res.*, *113*, C01005, doi:10.1029/2006JC004031.

Li, C., E. Weeks, and J. Rego (2009), In situ measurements of saltwater flux through tidal passes of Lake Pontchartrain Estuary by Hurricanes Gustav and Ike in September 2008, *Geophys. Res. Lett.*, *36*, L19609, doi:10.1029/2009GL039802.

McGee, B. D., B. B. Goree, R. W. Tollett, B. K. Woodward, and W. H. Kress (2006), Hurricane Rita surge data, southwestern Louisiana and southeastern Texas, September to November 2005, *U.S. Geol. Surv. Data Series*, *220*.

Mellor, G. L., and T. Yamada (1982), Development of a turbulence closure model for geophysical fluid problem, *Rev. Geophys.*, *20*, 851–875, doi:10.1029/RG020i004p00851.

Morey, S. L., S. Baig, M. A. Bourassa, D. S. Dukhovskoy, and J. J. O'Brien (2006), Remote forcing contribution to storm-induced sea level rise during Hurricane Dennis, *Geophys. Res. Lett.*, *33*, L19603, doi:10.1029/2006GL027021.

Mukai, A. Y., J. J. Westerink, R. A. Luettich Jr., and D. Mark (2002), Eastcoast 2001: A tidal constituent database for the western North Atlantic, Gulf of Mexico and Caribbean Sea, *Tech. Rep., ERDC/CHL TR-02-24*, 201 pp., Coastal and Hydraul. Lab., Eng. Res. and Dev. Cent., U.S. Army Corps of Eng., Vicksburg, Miss.

Peng, M., L. Xie, and L. J. Pietrafesa (2004), A numerical study of storm surge and inundation in the Croatan-Albemarle-Pamlico Estuary System, *Estuarine Coastal Shelf Sci.*, *59*(1), 121–137, doi:10.1016/j.ecss.2003.07.010.

Peng, M., L. Xie, and J. Pietrafesa (2006a), A numerical study on hurricane induced storm surge and inundation in Charleston, South Carolina, *J. Geophys. Res.*, *111*, C08017, doi:10.1029/2004JC002755.

Peng, M., L. Xie, and L. J. Pietrafesa (2006b), Tropical cyclone induced asymmetry of sea level surge and fall and its presentation in a storm surge model with parametric wind fields, *Ocean Modell.*, *14*, 81–101, doi:10.1016/j.ocemod.2006.03.004.

Powell, M. D., S. H. Houston, and T. A. Reinhold (1996), Hurricane Andrew's landfall in south Florida. Part I: Standardizing measurements for documentation of surface wind fields, *Weather Forecast.*, *11*, 304–328, doi:10.1175/1520-0434(1996)011<0304:HALISF>2.0.CO;2.

Proudman, J. (1955), The propagation of tide and surge in an estuary, *Proc. R. Soc. London, Ser. A*, *231*, 8–24, doi:10.1098/rspa.1955.0153.

Proudman, J. (1957), Oscillations of tide and surge in an estuary of finite length, *J. Fluid Mech.*, *2*, 371–382, doi:10.1017/S002211205700018X.

Pugh, D. T. (1987), *Tides, Surges and Mean Sea-Level: A Handbook for Engineers and Scientists*, 472 pp., John Wiley, Hoboken, N. J.

Pugh, D. T., and J. M. Vassie (1980), Applications of the joint probability method for extreme sea level computations, *Proc. Inst. Civ. Eng., Part 2*, *69*, 959–975, doi:10.1680/iicep.1980.2179.

Qin, Z., Y. Duan, Y. Wang, Z. Shen, and K. Xu (1994), Numerical simulation and prediction of storm surges and water levels in Shanghai harbour and its vicinity, *Nat. Hazards*, *9*, 167–188, doi:10.1007/BF00662597.

Rego, J. L. (2009), Storm surge dynamics over wide continental shelves: Numerical experiments using the finite-volume coastal ocean model, Ph.D. dissertation, 147 pp., La. State Univ., Baton Rouge.

Rego, J. L., and C. Li (2009a), On the importance of the forward speed of hurricanes in storm surge forecasting: A numerical study, *Geophys. Res. Lett.*, *36*, L07609, doi:10.1029/2008GL036953.

Rego, J. L., and C. Li (2009b), On the receding of storm surge along Louisiana's low-lying coast, *J. Coastal Res.*, *SI56*(2), 1045–1049.

Resio, D. T., and J. J. Westerink (2008), Modeling the physics of storm surges, *Phys. Today*, *61*(9), 33–38, doi:10.1063/1.2982120.

Retana, A. G. (2008), Salinity transport in a finite-volume sigma-layer three-dimensional model, Ph.D. thesis, 706 pp., Univ. of New Orleans, New Orleans.

Rossiter, J. R. (1961), Interaction between tide and surge in the Thames, *Geophys. J. R. Astron. Soc.*, *6*, 29–53.

Shen, J., and W. Gong (2009), Influence of model domain size, wind directions and Ekman transport on storm surge development inside the Chesapeake Bay: A case study of extratropical cyclone Ernesto, *J. Mar. Syst.*, *75*, 198–215.

Smagorinsky, J. (1963), General circulation experiments with the primitive equations. I: The basic experiment, *Mon. Weather Rev.*, *91*, 99–164, doi:10.1175/1520-0493(1963)091<0099:GCEWTP>2.3.CO;2.

Tang, Y. M., R. Grimshaw, B. Sanderson, and G. Holland (1996), A numerical study of storm surges and tides, with application to the north Queensland coast, *J. Phys. Oceanogr.*, *26*, 2700–2711, doi:10.1175/1520-0485(1996)026<2700:ANSOSS>2.0.CO;2.

URS Group (2006), Hurricane Rita rapid response: Louisiana coastal and riverine high water mark collection, contract EMW-2000-CO-0247, task orders 445 and 450, 42 pp., Hazard Mitigation Tech. Assistance Program, Fed. Emergency Manage. Agency, Gaithersburg, Md.

Weisberg, R. H., and L. Y. Zheng (2006a), Hurricane storm surge simulation for Tampa Bay, *Estuaries Coasts*, *29*(6), 899–913.

Weisberg, R. H., and L. Zheng (2006b), A simulation of the Hurricane Charley storm surge and its breach of North Captiva Island, *Fla. Sci.*, *69*, 152–165.

Weisberg, R. H., and L. Zheng (2008), Hurricane storm surge simulations comparing three-dimensional with two-dimensional formulations based on an Ivan-like storm over the Tampa Bay, Florida region, *J. Geophys. Res.*, *113*, C12001, doi:10.1029/2008JC005115.

Welander, P. (1961), Numerical predictions of storm surges, *Adv. Geophys.*, *8*, 315–379.

Wolf, J. (1978), Interaction of tide and surge in a semi-infinite uniform channel, with application to surge propagation down the east coast of Britain, *Appl. Math. Model.*, *2*, 245–253, doi:10.1016/0307-904X(78)90017-3.

Wolf, J. (1981), Surge-tide interaction in the North Sea and River Thames, in *Floods due to High Winds and Tides*, edited by Peregrine, D. H., pp. 75–94, Academic, London.

Wolf, J. (2009), Coastal flooding: Impacts of coupled wave–surge–tide models, *Nat. Hazards*, *49*(2), 241–260, doi:10.1007/s11069-008-9316-5.

Zhang, Y., Y. Zhao, and Y. Wang (1993), Analysis of disaster caused by typhoon surges and study of the numerical prediction methods for the disastrous sea level, in *Tropical Cyclone Disasters*, edited by Lighthill, J. et al., pp. 452–459, Peking Univ. Press, Beijing.

C. Li, Coastal Studies Institute, Department of Oceanography and Coastal Sciences, School of the Coast and Environment, Louisiana State University, Baton Rouge, LA 70803, USA. (cli@lsu.edu)

J. L. Rego, Division of Marine and Coastal Systems, Deltares, Rotterdamseweg 185, NL-2629 HD Delft, Netherlands. (joao.rego@deltares.nl)